

7.3 Multi-pulse models

In this section, we formulate one-dimensional models for the case where multiple heat pulses are applied to the boundary of a specimen. We show how the modal solutions for single-pulse models, as derived in Section 6.9, can be adapted to solve these multi-pulse models. As was the case with the single-pulse model, we will not develop a full, realistic mathematical model of an actual physical process, and we retain the assumption that all the heat is absorbed at the boundary at $x = 0$.

7.3.1 Multi-pulse problem for the C-V and DPL models

The multi-pulse problem is similar to the single-pulse problem, with the difference that the heat pulse is modelled using a step function with multiple pulse cycles for the temperature $T(0, t)$ at the boundary.

To simplify the formulation of the multi-pulse problem and also the implementation of our numerical calculations, we define a pulse cycle as a "pulse ON" followed by a "pulse OFF" event. The first "pulse ON" starts at $t = 0$ and stops at $t = t_1$. The first "pulse OFF" stops at $t = t_2$. To be consistent with laser terminology, the pulse width is $t_p = t_1$ and the pulse period is $\tau_p = t_2$ (*i.e.* the total duration of "pulse ON" and "pulse OFF"). For a pulse-train consisting of m pulse cycles, the boundary condition at $x = 0$ is given by

$$T(0, t) = \begin{cases} 1, & t_{n-1} \leq t < t_n \\ 0, & t_n \leq t < t_{n+1} \\ 0, & t \geq t_{2m} \end{cases} \quad (7.3.1)$$

with $t_0 = 0$ and $n = 1, 3, 5, \dots, (2m - 1)$.

Solving the multi-pulse problem for the first pulse cycle is done in the same way as for the C-V, DPL and Fourier model (refer to Sections 6.9.1 to 6.9.3). Note however that Problem 2 is formulated on a finite time interval. We use

the DPL model to illustrate the solution strategy:

$$\begin{aligned}
 \partial_t^2 T + 2\gamma \partial_t T - \tau_T c^2 \partial_t \partial_x^2 T &= c^2 \partial_x^2 T & (7.3.2) \\
 T(0, t) &= \begin{cases} 1, & t_{n-1} \leq t < t_n \\ 0, & t_n \leq t < t_{n+1} \\ 0, & t \geq t_{2m} \end{cases} \\
 \partial_x T(1, t) &= 0 \\
 T(x, 0) &= 0 \\
 \partial_t T(x, 0) &= 0
 \end{aligned}$$

where $2\gamma = 1/\tau_q$, $c^2 = \alpha/\tau_q$ and t_p is the pulse width. To solve this model, we start by considering the time interval $0 \leq t < t_p$ and use the notation $T_1(x, t)$ for the temperature $T(x, t)$ restricted to this interval.

Problem 1 ("pulse ON"): $T_1(0, t) = 1 \quad (0 \leq t < t_1 = t_p)$

To use the separation of variables method, we need to homogenize the boundary value by setting $u_1(x, t) = 1 - T_1(x, t)$ and then solve the equivalent problem (Problem 1) for $u_1(x, t)$. Problem 1 is formulated as

$$\begin{aligned}
 \partial_t^2 u_1 + 2\gamma \partial_t u_1 - \tau_T c^2 \partial_t \partial_x^2 u_1 &= c^2 \partial_x^2 u_1, \quad 0 < x < 1, \quad 0 < t < t_p & (7.3.3) \\
 u_1(0, t) &= 0 \\
 \partial_x u_1(1, t) &= 0 \\
 u_1(x, 0) &= 1 \\
 \partial_t u_1(x, 0) &= 0.
 \end{aligned}$$

As in Section 6.9.2, the solution for Problem 1 is given by $T_1(x, t) = 1 - u_1(x, t)$, for $0 \leq t < t_1$, where $u_1(x, t)$ is the solution of the homogenized problem. The series representation of $u_1(x, t)$ is derived in Sections 6.2.2 to 6.2.5 using modal analysis.

Remark: In the remainder of this section, we show that the solutions of all further subproblems can be expressed in terms of the function $u_1(x, t)$. This is a key feature of the methodology used for simulating temperature profiles for the multi-pulse problems.

Problem 2 ("pulse OFF"): $T_2(0, t) = 0 \quad (t_1 \leq t < t_2 = \tau_p)$

We denote the solution to Problem 2 by $T_2(x, t)$. The values for $T_1(x, t_1)$ and $\partial_t T_1(x, t_1)$ now become the initial conditions for Problem 2.

As in Sections 6.9.1 and 6.9.2, Problem 2 is formulated as

$$\begin{aligned}
 \partial_t^2 T_2 + 2\gamma \partial_t T_2 - \tau_T c^2 \partial_t \partial_x^2 T_2 &= c^2 \partial_x^2 T_2 & (7.3.4) \\
 T_2(0, t) = \partial_x T_2(1, t) &= 0 \\
 T_2(x, t_1) &= T_1(x, t_1) = 1 - u_1(x, t_1) \\
 \partial_t T_2(x, t_1) &= \partial_t T_1(x, t_1) = -\partial_t u_1(x, t_1)
 \end{aligned}$$

To solve for $T_2(x, t)$ we use $u_1(x, t)$ for $t \geq t_1$ and define $Q_1(x, t) = T_2(x, t) + u_1(x, t)$. Then $T_2(x, t) = Q_1(x, t) - u_1(x, t)$ satisfies Eq. (7.3.4) and $Q_1(x, t)$ is the solution of

$$\begin{aligned}
 \partial_t^2 Q_1 + 2\gamma \partial_t Q_1 - \tau_T c^2 \partial_t \partial_x^2 Q_1 &= c^2 \partial_x^2 Q_1 & (7.3.5) \\
 Q_1(0, t) = \partial_x Q_1(1, t) &= 0 \\
 Q_1(x, t_1) &= 1 \\
 \partial_t Q_1(x, t_1) &= 0
 \end{aligned}$$

Equation (7.3.5) is the same as Eq. (7.3.3), except that the initial conditions are specified at $t = t_1$. From the linearity of the partial differential equation, it consequently follows that for $t \geq t_1$, $Q_1(x, t) = u_1(x, t - t_1)$ and therefore

$$T_2(x, t) = u_1(x, t - t_1) - u_1(x, t), \quad (7.3.6)$$

or, alternatively,

$$T_2(x, t) = T_1(x, t) + u_1(x, t - t_1) - 1. \quad (7.3.7)$$

The function $T_2(x, t)$ is the solution for Problem 2 for $t_1 \leq t < t_2$, but as the function $T_2(x, t)$ is defined for all t it can be used in the expressions for the solutions associated with the subsequent pulses.

For the second pulse cycle, as for the first cycle, two subproblems, Problem 3 and Problem 4, are considered for the "pulse ON" and "pulse OFF" events.

Problem 3 ("pulse ON"): $T_3(0, t) = 1$ ($t_2 \leq t < t_3 = \tau_p + t_p$)

The values for $T_2(x, t_2)$ and $\partial_t T_2(x, t_2)$ are the starting values for Problem 3:

$$\begin{aligned}
 \partial_t^2 T_3 + 2\gamma \partial_t T_3 - \tau_T c^2 \partial_t \partial_x^2 T_3 &= c^2 \partial_x^2 T_3 & (7.3.8) \\
 T_3(0, t) &= 1 \\
 \partial_x T_3(1, t) &= 0 \\
 T_3(x, t_2) &= T_2(x, t_2) = u_1(x, t_2 - t_1) - u_1(x, t_2) \\
 \partial_t T_3(x, t_2) &= \partial_t u_1(x, t_2 - t_1) - \partial_t u_1(x, t_2)
 \end{aligned}$$

To homogenize this problem, we set

$$T_3(x, t) = 1 - u_2(x, t).$$

Problem 3 is equivalent to

$$\begin{aligned} \partial_t^2 u_2 + 2\gamma \partial_t u_2 - \tau_T c^2 \partial_t \partial_x^2 u_2 &= c^2 \partial_x^2 u_2 & (7.3.9) \\ u_2(0, t) &= 0 \\ \partial_x u_2(1, t) &= 0 \\ u_2(x, t_2) &= 1 - [u_1(x, t_2 - t_1) - u_1(x, t_2)] \\ \partial_t u_2(x, t_2) &= -[\partial_t u_1(x, t_2 - t_1) - \partial_t u_1(x, t_2)] \end{aligned}$$

To solve for $u_2(x, t)$ we continue using $T_2(x, t)$ for $t \geq t_2$ and define $Q_2(x, t) = u_2(x, t) + T_2(x, t)$.

Then $Q_2(x, t)$ is a solution of

$$\begin{aligned} \partial_t^2 Q_2 + 2\gamma \partial_t Q_2 - \tau_T c^2 \partial_t \partial_x^2 Q_2 &= c^2 \partial_x^2 Q_2 & (7.3.10) \\ Q_2(0, t) = \partial_x Q_2(1, t) &= 0 \\ Q_2(x, t_2) &= 1 \\ \partial_t Q_2(x, t_2) &= 0 \end{aligned}$$

and can be expressed in terms of $u_1(x, t)$.

For $t_2 \leq t < t_3$:

$$\begin{aligned} u_2(x, t) &= Q_2(x, t) - T_2(x, t) \\ &= u_1(x, t - t_2) - [u_1(x, t - t_1) - u_1(x, t)] \end{aligned}$$

The solution for Problem 3 is given by

$$T_3(x, t) = 1 - \{u_1(x, t - t_2) - [u_1(x, t - t_1) - u_1(x, t)]\}, \quad (7.3.11)$$

or, alternatively,

$$T_3(x, t) = 1 - u_1(x, t - t_2) + T_2(x, t). \quad (7.3.12)$$

Problem 4 ("pulse OFF"): $T_4(0, t) = 0$ ($t_3 \leq t < t_4 = 2\tau_p$)

We denote the solution of Problem 4 by $T_4(x, t)$. The values for $T_3(x, t_3)$ and $\partial_t T_3(x, t_3)$ become the initial conditions for Problem 4:

$$\begin{aligned} \partial_t^2 T_4 + 2\gamma \partial_t T_4 - \tau_T c^2 \partial_t \partial_x^2 T_4 &= c^2 \partial_x^2 T_4 & (7.3.13) \\ T_4(0, t) = \partial_x T_4(1, t) &= 0 \\ T_4(x, t_3) &= T_3(x, t_3) = 1 - u_2(x, t_3) \\ &= 1 - \{u_1(x, t_3 - t_2) - [u_1(x, t_3 - t_1) - u_1(x, t_3)]\} \\ \partial_t T_4(x, t_3) &= \partial_t T_3(x, t_3) = -\partial_t u_2(x, t_3) \\ &= -\{\partial_t u_1(x, t_3 - t_2) - [\partial_t u_1(x, t_3 - t_1) - \partial_t u_1(x, t_3)]\} \end{aligned}$$

As before, to solve for $T_4(x, t)$ we continue using $u_2(x, t)$ for $t \geq t_3$ and define $Q_3(x, t) = T_4(x, t) + u_2(x, t)$.

Then $T_4(x, t) = Q_3(x, t) - u_2(x, t)$ will satisfy Eq. (7.3.13) and $Q_3(x, t)$ is the solution of

$$\begin{aligned} \partial_t^2 Q_3 + 2\gamma \partial_t Q_3 - \tau_T c^2 \partial_t \partial_x^2 Q_3 &= c^2 \partial_x^2 Q_3 & (7.3.14) \\ Q_3(0, t) = \partial_x Q_3(1, t) &= 0 \\ Q_3(x, t_3) &= 1 \\ \partial_t Q_3(x, t_3) &= 0 \end{aligned}$$

For $t \geq t_3$, $Q_3(x, t) = u_1(x, t - t_3)$ and it follows that

$$T_4(x, t) = u_1(x, t - t_3) - \{u_1(x, t - t_2) - [u_1(x, t - t_1) - u_1(x, t)]\}, \quad (7.3.15)$$

or

$$T_4(x, t) = T_3(x, t) + u_1(x, t - t_3) - 1. \quad (7.3.16)$$

The solutions for Problems 1 to 4 can be summarised as:

$$\begin{aligned} T_1(x, t) &= 1 - u_1(x, t) & (t_0 \leq t < t_1) \\ T_2(x, t) &= T_1(x, t) + u_1(x, t - t_1) - 1 & (t_1 \leq t < t_2) \\ T_3(x, t) &= 1 - u_1(x, t - t_2) + T_2(x, t) & (t_2 \leq t < t_3) \\ T_4(x, t) &= T_3(x, t) + u_1(x, t - t_3) - 1 & (t_3 \leq t < t_4) \end{aligned}$$

For a pulse train with m pulse cycles the solution is given by a sequence of functions

$$T_n(x, t) = 1 - u_1(x, t - t_{n-1}) + T_{n-1}(x, t) \quad (t_{n-1} \leq t < t_n) \quad (7.3.17)$$

$$T_{n+1}(x, t) = T_n(x, t) + u_1(x, t - t_n) - 1 \quad (t_n \leq t < t_{n+1})$$

for $n = 1, 3, 5, \dots, 2m - 1$.

Note that $T_0(x, 0) = 0$ and that $T_{2m}(x, t)$ is defined for $t \geq t_{2m-1}$.

For the multi-pulse problem for the C-V model, set $\tau_T = 0$ in Eq. (7.3.2) and all subsequent problems.

7.3.2 Multi-pulse problem for the Fourier model

We solve the multi-pulse problem for the Fourier model in the same way as the C-V and DPL models, even though the partial differential equation is a

diffusion equation. For the multi-pulse problem, the boundary condition at $x = 0$ for the single-pulse problem (Eq. (6.9.8)), has to be adapted, similar to Eq. (7.3.1), so that the multi-pulse Fourier model is given by

$$\begin{aligned}
 \partial_t T &= \alpha \partial_x^2 T & (7.3.18) \\
 T(0, t) &= \begin{cases} 1, & t_{n-1} \leq t < t_n \\ 0, & t_n \leq t < t_{n+1} \\ 0, & t \geq t_{2m} \end{cases} \\
 \partial_x T(1, t) &= 0 \\
 T(x, 0) &= 0
 \end{aligned}$$

with $t_0 = 0$ and $n = 1, 3, 5, \dots (2m - 1)$.

Problem 1 ("pulse ON"): $T_1(0, t) = 1 \quad (0 \leq t < t_1)$

As before, the problem is homogenized by setting $u_1(x, t) = 1 - T_1(x, t)$. This problem is solved using separation of variables, and $T_1(x, t) = 1 - u_1(x, t)$ is the solution for Eq. (7.3.18) when $0 \leq t < t_1$. The series representation for $u_1(x, t)$ is derived in Section 6.2.5.

Problem 2 ("pulse OFF"): $T_1(0, t) = 0 \quad (t_1 \leq t < t_2)$

We denote the solution to Problem 2 by $T_2(x, t)$. The value for $T_1(x, t_1)$ is the initial condition for Problem 2.

Problem 2 is formulated as

$$\begin{aligned}
 \partial_t T_2 &= \alpha \partial_x^2 T_2 & (7.3.19) \\
 T_2(0, t) = \partial_x T_2(1, t) &= 0 \\
 T_2(x, t_1) &= T_1(x, t_1) = 1 - u_1(x, t_1)
 \end{aligned}$$

As before, to solve for $T_2(x, t)$ we use $u_1(x, t)$ for $t \geq t_1$. We define $Q_1(x, t) = T_2(x, t) + u_1(x, t)$. Then $T_2(x, t) = Q_1(x, t) - u_1(x, t)$ satisfies Eq. (7.3.19).

$Q_1(x, t)$ is the solution of

$$\begin{aligned}
 \partial_t Q_1 &= \alpha \partial_x^2 Q_1 & (7.3.20) \\
 Q_1(0, t) = \partial_x Q_1(1, t) &= 0 \\
 Q_1(x, t_1) &= 1
 \end{aligned}$$

For $t \geq t_1$, $Q_1(x, t) = u_1(x, t - t_1)$ and it follows that

$$T_2(x, t) = u_1(x, t - t_1) - u_1(x, t). \quad (7.3.21)$$

The solution for the subsequent pulse cycles are derived in the same way as in Section 7.3.1 and are given by Eq. (7.3.17).

7.3.3 Series solution

For the numerical investigation of the multi-pulse problem, the series representation of the solutions $u_1(x, t)$ for the Fourier, C-V and DPL models are required. This section contains a short summary of these series representations as derived in Section 6.2.

All three models have the same associated eigenvalue problem, and the eigenfunctions (normalised with respect to the norm of the square integrable functions) are given by

$$w_k(x) = \sin \nu_k x \quad \text{with } \nu_k = \frac{(2k-1)\pi}{2} \quad \text{for } k = 1, 2, \dots \quad (7.3.22)$$

The series representation for the solution $u_1(x, t)$ follows as

$$u_1(x, t) = \sum_{k=1}^{\infty} y_k(t) w_k(x) \quad (7.3.23)$$

where $y_k(t)$ must be determined for each of the three models. The initial condition $u_1(x, 0) = 1$ is used for all three models, and it is easy to check that

$$y_k(0) = \int_0^1 u_1(0, t) w_k(x) dx = \frac{2}{\nu_k}. \quad (7.3.24)$$

The additional initial condition $\partial_t u_1(x, 0) = 0$, yielding $y'_k(0) = 0$ is required for the C-V and DPL models.

Fourier model:

We solve first order linear differential equations to find

$$y_k(t) = \frac{\sqrt{2}}{\nu_k} e^{-r_k t} \quad \text{with } r_k = \alpha \nu_k^2. \quad (7.3.25)$$

DPL model:

The DPL model is a second order hyperbolic differential equation, and we use the terminology from vibration analysis to describe properties of the eigenfunctions (or modes). We introduce the notation $\gamma_k = \gamma + \tau_T c^2 \nu_k^2$ and consider two cases for the modes: the overdamped case ($\gamma_k^2 > c^2 \nu_k^2$) and the underdamped case ($\gamma_k^2 < c^2 \nu_k^2$).

In the overdamped case, let $r_1^k = -\gamma_k + \sqrt{\gamma_k^2 - c^2 \nu_k^2}$, $r_2^k = -\gamma_k - \sqrt{\gamma_k^2 - c^2 \nu_k^2}$ and $r_k = r_2^k / r_1^k$. Then

$$y_k(t) = a_k \left(e^{r_1^k t} - \frac{1}{r_k} e^{r_2^k t} \right) \quad \text{with } a_k = -\frac{\sqrt{2} r_k}{\nu_k (1 - \nu_k)}. \quad (7.3.26)$$

In the underdamped case, let $\omega_k^d = \sqrt{c^2\nu_k^2 - \gamma_k^2}$. Then

$$y_k(t) = c_k e^{-\gamma_k t} \left(\cos \omega_k^d t + \frac{\gamma_k}{\omega_k^d} \sin \omega_k^d t \right) \quad \text{with } c_k = \frac{\sqrt{2}}{\nu_k}. \quad (7.3.27)$$

When computing the series solution in Eq. (7.3.23) for the DPL model it must be checked for each k , whether Eq. (7.3.26) or Eq. (7.3.27) applies.

For the DPL model the constitutive equation is given by

$$q(x, t + \tau_q) = -\partial_x T(x, t + \tau_T),$$

where q is the heat flux and $\partial_x T$ the temperature gradient. A linear approximation of this constitutive equation is used to derive the model. For the numerical simulations in Sections 7.4 to 7.6, we distinguish between two cases. For $0 < \tau_T < \tau_q$, the temperature gradient precedes the heat flux vector [Tzo97]. We refer to this case as DPL-I. In this case, the first modes are overdamped, followed by some underdamped modes, and then all the remaining modes are overdamped. For $0 < \tau_q < \tau_T$ the temperature gradient follows after the heat flux vector. We refer to this case as DPL-II, and note that all the modes are overdamped. The case where $\tau_T = \tau_q$, is a special case, and in [Tzo97, Section 2.5] Tzou identifies this as a case where heat transfer occurs by diffusion. We include this special case with DPL-II, as all the modes are overdamped. It is convenient to define $\delta \equiv \tau_T/\tau_q$ – then $0 < \delta < 1$ indicates the DPL-I model and $\delta \geq 1$ indicates the DPL-II model. For the special case where $\delta = 1$, we expect the DPL-II model to display diffusive behaviour, i.e. similar to the Fourier model.

C-V model:

For the C-V model, we choose $\tau_T = 0$ in Eq. (7.3.26) and Eq. (7.3.27). This means that $\gamma_k = \gamma$ for all k .

For the C-V model, the first modes are overdamped, but all higher modes are underdamped at the same rate $e^{-\gamma t}$.

7.3.4 Parameter values for numerical investigation

The first issue is to decide on the number of terms n to use for the finite sum approximations for $u_1(x, t)$. In the simulations we use the discontinuous initial condition $u_1(x, 0) = 1$. Recall that this is the same initial condition used in the continuous and single-pulse heating cases in Chapter 6. We therefore follow the same procedure as described in Section 6.5. We use error

estimates as a guideline for the relative approximation error and determine the number of modes n by deciding on an acceptable relative approximation error. For $n = 3000$ modes, the relative approximation error (in the norm of the square integrable functions) is less than 4×10^{-5} , and we will use this value in most of the simulations. Note that the required number of modes does not depend on the values of the parameters α , τ_q and τ_T , as these parameters do not appear in the eigenfunctions.

Secondly, the value for the dimensionless thermal diffusivity α^* is required, which depends on t_0 , the time scaling factor for the dimensionless time variable. For the simulations in Section 7.4, we use the value for t_0 as chosen for the continuous and single-pulse simulations in Chapter 6. This allows for easy comparison with the multi-pulse problems. We recall from Section 2.8.1 that at t_0 , the fundamental modal solution for the Fourier model has decreased by 1%. We have

$$t_0 = -\frac{4 \ln(0.99)d^2}{\pi^2\alpha} \approx 0.0040732 \frac{d^2}{\alpha} \quad (7.3.28)$$

and consequently, the dimensionless thermal diffusivity follows as

$$\alpha^* = \frac{t_0\alpha}{d^2} = 0.0040732. \quad (7.3.29)$$

It is easy to use a different reference time t_0 . In Section 7.5, for simulations linked to a thermorefectance example, we use the diffusion time t_d as reference time. In this case,

$$t_0 = t_d = \frac{d^2}{\alpha} \text{ with } \alpha^* = 1. \quad (7.3.30)$$

In Section 7.6, we consider bio-heat applications and use the half-time $t_{1/2}$ as reference time which yields

$$t_0 = t_{1/2} = \frac{d^2}{\alpha} \text{ with } \alpha^* = 0.1388. \quad (7.3.31)$$

In all cases, due to the choice of t_0 , the value for α^* is independent of the specimen thickness d and the thermal diffusivity α .

Thirdly, values for the dimensionless lag times τ_q^* and τ_T^* are required. In Sections 6.3 and 6.7 we derive upper bounds,

$$\tau_q^* \leq \frac{\varepsilon}{\alpha^*\pi^2} \quad \text{and} \quad \tau_T^* \leq \frac{4\varepsilon}{\alpha^*\pi^2} \quad (7.3.32)$$

for the lag times, with $\varepsilon \ll 1$ a user specified accuracy. Using $\varepsilon = 0.001$, we obtain the value $\tau_q^* = 0.024875$. The value for τ_T^* is chosen in such a way that sensible comparisons between the DPL and C-V models are possible. We obtain $\tau_T^* = 0.0041782$ for the DPL-I model, and $\tau_T^* = \tau_q^* = 0.024875$ for the DPL-II model. These values for the lag times are used in Section 7.4.

For the numerical investigations related to the thermorefectance example in Section 7.5 and the bio-heat application in Section 7.6, we seek values of the lag times that result in distinct differences between the different model predictions. When deciding on the values for τ_q^* and τ_T^* , we ensure that values remain within an acceptable range. The upper bounds given in Eq. (7.3.32) are used, however, ε has to be specified in a consistent and realistic way. This is done by choosing a value for ε , finding r_1^I and r_1^F respectively, and calculating the percentage fractional difference $100 \times |(r_1^F - |r_1^I|)/r_1^F|$. We decide on a maximum allowable percentage of approximately 10% and consistently use this value to ensure that for each choice of ε , the values for τ_q^* and τ_T^* remain within an acceptable range.

7.4 Comparison with single-pulse problem

In the remaining sections all variables and parameters are dimensionless and, for convenience, we return to using the original notation. Where physical parameters are referred to, it will be clear from the context, and the units are given.

Our investigation of the multi-pulse problem starts by finding the solutions for the Fourier, C-V and DPL models with the values for the dimensionless parameters as in Section 6.9, so that the single-pulse problems and the multi-pulse problems can be compared. These parameter values are: $\alpha = 0.0040732$, $\tau_q = 0.024875$, $\tau_T^I = 0.0041782$ (DPL-I model) and $\tau_T^{II} = \tau_q = 0.024875$ (DPL-II model). In this case $\delta^{II} = 1$. We use finite sum approximations of the series solutions, with $n = 3000$ modes, to find temperature distributions. These temperature profiles are temporally calculated at a fixed position in the specimen over time. In particular, we investigate the effects of changing the pulse period τ_p and the number m of pulse cycles in the pulse-train on the solutions.

Before starting with the investigation, we want to determine how accurately the temperature pulse mimics the incident heat pulse, at positions close to $x = 0$. In Section 6.10.4 we mention that at positions close to the $x = 0$ boundary, it is necessary to increase the number of modes n to ensure

accurate predictions. We find through experimentation that at $x = 0.001$, at least $n = 30000$ modes are required to ensure an accurate solution. Figure 7.1, with the pulse width $t_p = 0.075$ and the pulse period $\tau_p = 0.15$, shows that for all the models, except the DPL-II model, the temperature profile closely resembles the incident step heat pulse. The DPL-II temperature profile gradually ramps up, reaches a slightly lower maximum temperature value, and gradually decreases again. This deviation from the step pulse is expected considering the strong damping built into the DPL-II model.

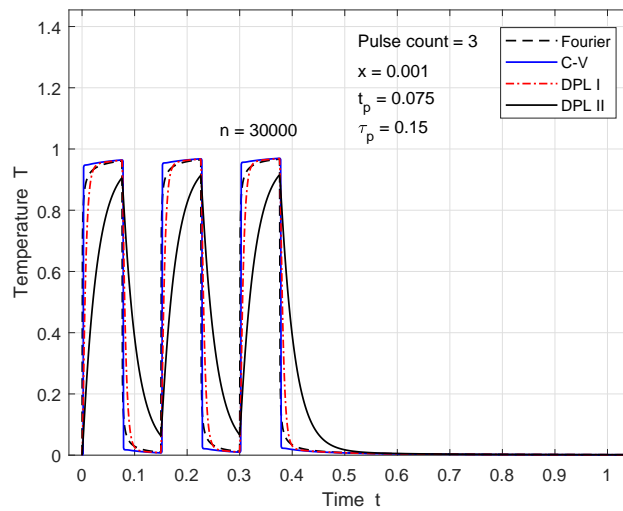


Figure 7.1: Temperature profiles at $x = 0.001$, close to the boundary

Figure 7.2 shows the temperature profiles for a three-pulse problem, calculated at a fixed position $x = 0.02$. The C-V temperature profile is characterised by sharp thermal wave fronts, that distinguish it from the profiles of the other models. Small amplitude Gibbs oscillations are present near these sharp wave fronts. (Using more modes reduces the amplitude of the Gibbs oscillations; this is also true near the discontinuities.)

The instant when the temperature at $x = 0.02$ starts to rise, also differs for the respective models. The Fourier and DPL-II models predict an immediate rise in temperature, followed by the DPL-I model. The C-V model however predicts a fairly long delay, compared to the other models, followed by a sudden jump in the temperature at the arrival of the thermal wave front. As expected, the temperature profiles for the first pulse cycle agree with the profiles for the single-pulse models in Figure 6.25.

Similar for each model, is the increase in the peak temperature value with each consecutive pulse. This is to be expected since the temperature does

not decrease to its original zero level before the next pulse is incident on the specimen. The most noticeable difference between the models is the difference in predicted peak temperatures. The highest temperatures are predicted by the C-V model, followed by the DPL-I, then Fourier, and lastly the DPL-II model. The difference does however reduce with each consecutive pulse. The time t at which the peak temperatures are reached also differ according to the model used. From first to last we have the Fourier, DPL-II, DPL-I and C-V model.

As anticipated, a sufficiently long time after the final pulse, the temperatures predicted by the four models are equal.

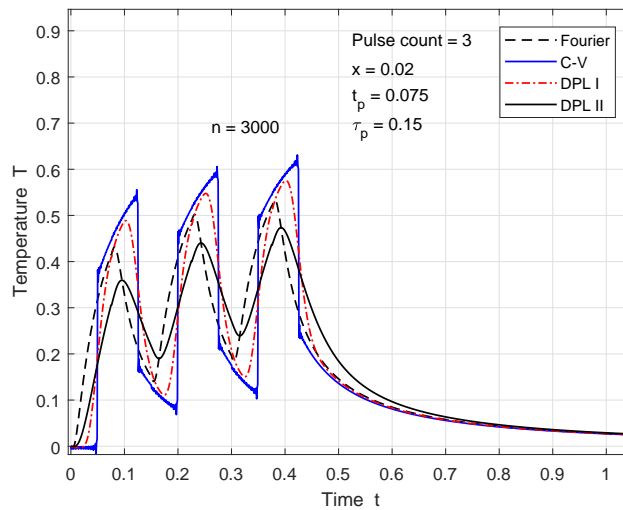


Figure 7.2: Temperature profiles at $x = 0.02$ for 3-pulse problem

Another interesting observation is obtained by choosing the fixed position x deeper into the specimen. Calculating the temperature profiles at say $x = 0.075$ (Figure 7.3) shows that the three pulses are starting to merge. However, the merging effect is less for the DPL-I model, and for the C-V model three distinct pulses are still clearly visible.

These properties of the temperature profiles agree with the physics of heat transfer. In the derivation of the heat transfer models in Section 6.9.1, we assume that all the optical energy is absorbed at $x = 0$. The absorbed energy increases the internal energy of the heat carriers in the surface region of the specimen. Initially, the gradient is small and therefore the diffusion of energy from the surface to the interior is slow. This results in a swift temperature rise in the surface region. Through interaction between the heat carriers,

the temperature gradient gradually increases with time, thereby promoting diffusion of energy from the surface to the interior. The diffusion process is slower than the absorption and the distinction between individual pulses becomes less with increasing x . The heat energy is distributed throughout the specimen resulting in a temperature level that is lower than the initial level in the surface region ([SYS07] [Yil12]).

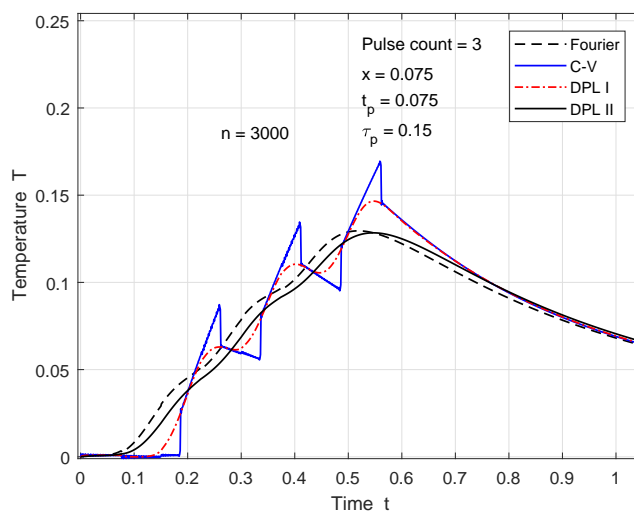


Figure 7.3: Temperature profiles at $x = 0.075$ showing merging of pulses

Next we investigate the effect of the pulse period on the temperature profiles. In Section 6.8 (Figures 6.10 and 6.13) it is shown that for the single-pulse problem, the four models predict the same temperatures from about $t = 0.35$. To determine the effect of the pulse period τ_p on the model predictions, we therefore increase the pulse period τ_p to 0.35, while keeping the pulse width unchanged at $t_p = 0.075$. The reason for this choice is to determine the effect when enough time elapses between consecutive pulses, for the temperature to return to zero before the next pulse starts. We then compare the temperature profiles at $x = 0.02$ with those in Figure 7.2 where $\tau_p = 0.15$.

Two properties are worth mentioning. Firstly, for the longer pulse period, the peak pulse heights increase at a slower rate. This is to be expected since more time is available for the temperature to decrease to a lower level before the arrival of the next pulse. We see in Figure 7.4 that all four models predict approximately the same temperature when the next pulse arrives, i.e. temperature values are within about 3% of each other. In Figure 7.2 there are still significant differences between the model predictions when the next pulse arrives. Secondly, the solutions of the Fourier and DPL-I models start

to agree well before the arrival of the next pulse. This agreement between the solutions of these two models did not occur for the case $\tau_p = 0.15$ in Figure 7.2. The pulse period τ_p also has an effect on the merging of individual

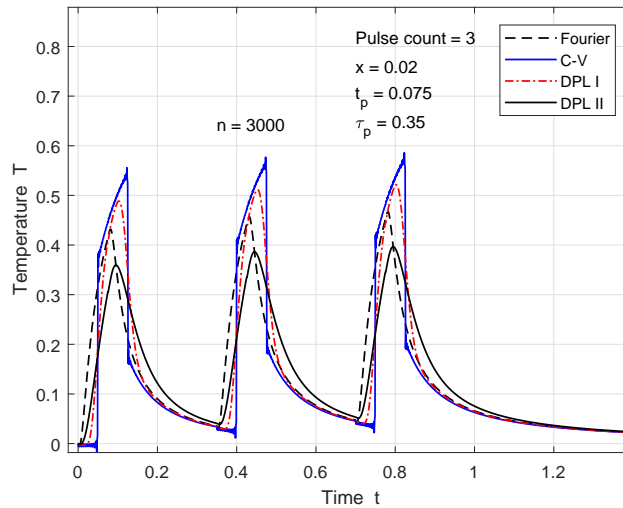


Figure 7.4: Temperature profiles at $x = 0.02$ with increased pulse period $\tau_p = 0.35$

pulses. Repeating the calculation with the same parameters as for Figure 7.3, but increasing the pulse period to $\tau_p = 0.35$ ($r_d = 0.075/0.35 = 0.214$), we see that the merging is reduced, and that three distinct temperature pulses are visible for all four temperature profiles (Figure 7.5). The peak pulse heights are also lower, compared to Figure 7.3. At a fixed point x deeper into the specimen, merging of the pulses will again be more prominent.

Next, we want to investigate the effect of increasing the number of pulses m . In Figure 7.4, we have $t_p = 0.075$ and $\tau_p = 0.35$. For three pulses, the heating duration is $2\tau_p + t_p = 0.775$. If the pulse period is reduced to $\tau_p = 0.175$ whilst keeping t_p fixed, the duty ratio is doubled ($r_d = 0.075/0.175 = 0.429$). To keep the heating duration unchanged, we increase the number of pulses from $m = 3$ to $m = 5$.

Using the DPL-I profile as reference we see that the maximum temperature has increased from $T \approx 0.52$ in the 3-pulse case (Figure 7.4) to $T \approx 0.59$ in the 5-pulse case (Figure 7.6). The other models show similar behaviour. This is due to the higher duty ratio for the 5-pulse case, implying that more heat energy is injected into the specimen during the heating stage. The increase in peak temperature per pulse is higher in the 5-pulse case.

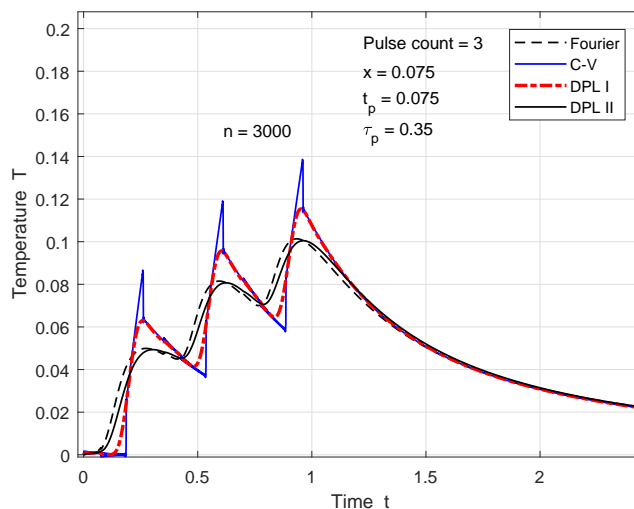


Figure 7.5: Merging of peaks at $x = 0.075$ with increased pulse period $\tau_p = 0.35$

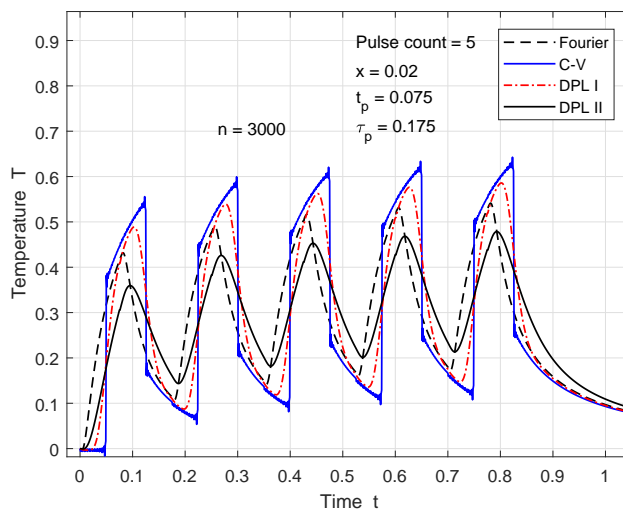


Figure 7.6: Temperature profiles at $x = 0.02$ for 5-pulse problem with fixed heating duration

If we do not restrict the heating duration and increase the number of pulses to $m = 20$, with $t_p = 0.075$ and $\tau_p = 0.175$, the peak temperatures gradually ramp up as shown in Figure 7.7. For instance, the peak temperatures for the DPL-I solution reaches a plateau value of $T \approx 0.63$, which is not much higher than the maximum after 5 pulses shown in Figure 7.6.

7.5. THERMOREFLECTANCE CASE STUDY: LOW DUTY RATIO r_d 151

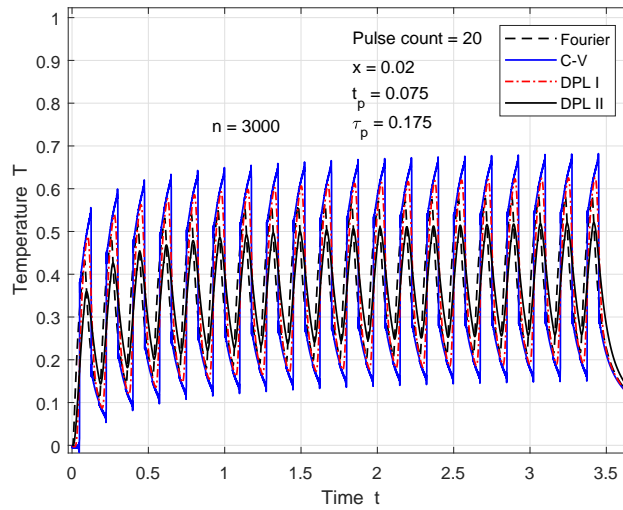


Figure 7.7: Temperature profiles at $x = 0.02$ for 20-pulse problem; reaching a plateau

Increasing the pulse period τ_p while keeping the pulse width t_p unchanged, decreases the duty ratio r_d . Decreasing r_d reduces the heat energy injected into the specimen, and will lead to lower peak temperatures and lower plateau values. We illustrate this effect with examples based on bio-heating in Section 7.6.

All the previous temperature profiles are calculated at a fixed point x in the interior of the specimen. In some applications the spatial temperature distribution is required, and in particular, the effect of the number of pulses on the temperature profile is of importance. The modal series solutions can be used to find spatial temperature distributions across the specimen at a fixed time t . This will be discussed in Section 7.6.

7.5 Thermorefectance case study: low duty ratio r_d

The case we investigate here relates to femtosecond thermorefectance experiments carried out on metal thin films. See, for instance, [Tzo97] and [Bro90] for early contributions. In a typical setup the front face is heated by the laser, while the rear surface is probed to determine the change in reflection, from which the change in temperature is determined. We choose a gold

thin film specimen with thickness $d = 50$ nm, and with thermal diffusivity $\alpha = 1.2495 \times 10^{-4} \text{ m}^2\text{s}^{-1}$. A typical laser pulse width is $t_p = 0.1$ ps.

For the dimensionless models, the front face is at $x = 0$ and the rear face at $x = 1$. For this example, we use the diffusion time as the time scaling factor, with $t_0 = t_d = d^2/\alpha = 20$ ps. The diffusion time is a concept that is well-known within the international materials metrology community, concerned with the measurement of thermophysical properties of materials ([BTY11][Bab10]), and it is easy to accommodate this different time scaling factor in the modal series solutions.

The following values are obtained for the dimensionless parameters with the new time scaling. Using Eq. (7.3.29) we calculate the dimensionless thermal diffusivity as $\alpha = 1$. The dimensionless pulse width is given by $t_p = 0.1/20 = 0.005$. The pulse period $\tau_p = 5$ is chosen to ensure that, for each model, subsequent pulse heights at a fixed interior point are almost equal. This means that the duty ratio is therefore $r_d = t_p/\tau_p = 0.001$.

The aim in this section is to study numerical examples where, at least initially, there is a distinct difference between the different model predictions. The lag times are determined by experimentation in order to achieve this. The experimentation is done using Eq. (7.3.32), with $\varepsilon = 0.125$ and checking that the percentage fractional difference $100 \times |(r_1^F - r_1^I)/r_1^F|$, introduced in Section 7.3.4, remains less than 10%.

The values $\tau_q = 0.012665$, $\tau_T^I = 0.002868$ (DPL-I model) and $\tau_T^{II} = 0.037995$ (DPL-II model) are obtained. We have the lag time ratios $\delta^I = \tau_T^I/\tau_q = 0.22645$ and $\delta^{II} = \tau_T^{II}/\tau_q = 3.0$. These lag time values are used in Figures 7.8 to 7.10. We focus on two aspects: the characteristics of the temperature pulses, specifically the pulse width and pulse height behaviour, and the effect of values used for the lag times, τ_q and τ_T , and consequently δ .

7.5.1 Characteristics of temperature pulses and wave fronts

Figure 7.8 shows the solutions for the four models, for three pulse cycles. Due to the low duty ratio (*i.e.* $r_d \ll 1$) no merging of pulses is observed. Three distinct pulses are predicted to reach the rear face at $x = 1$. Since the pulse period τ_p is long enough, the temperatures decrease to almost the same near zero value for all four the models before the next pulse starts. Subsequent pulses are therefore almost identical. The most noticeable feature of the temperature profile is the relatively high peak heights, and the narrow

7.5. THERMOREFLECTANCE CASE STUDY: LOW DUTY RATIO r_d 153

peak widths (although not clearly visible in the figure) of the C-V model compared to the other three models.

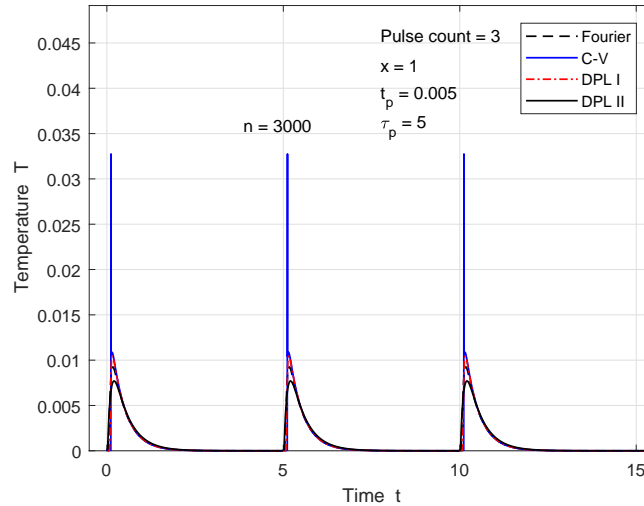


Figure 7.8: Temperature T at $x = 1$ showing 3 almost identical pulses. $\tau_q = 0.012665$; $\tau_T^I = 0.002868$ ($\delta^I = 0.2265$); $\tau_T^{II} = 0.037995$ ($\delta^{II} = 3$)

In Figure 7.9 we display the solutions for the first pulse only (observed at $x = 1$), in order to investigate the distinction between the different models in more detail. The DPL-I model predicts a pulse height higher than the Fourier model and the DPL-II model a pulse height lower than the Fourier model. The C-V model predicts a pulse more than three times the height of the DPL-I model. We also see that the DPL-II model predicts that the pulse arrives at $x = 1$ earlier, than for the Fourier model, and that the C-V model predicts the longest delay. To the right of the wave front, the C-V model coincides almost perfectly with the DPL-I model. After reaching their respective maximum temperatures, the model predictions coincide from $t \approx 0.4$. We can assume that from this time onwards, up to the start of the next pulse cycle, the transfer of heat in the specimen occurs by diffusion.

The maximum temperature values are relatively low at $x = 1$, *i.e.* $\sim 10^{-2}$. Compared to the boundary condition $T(0, t) = 1$, this implies an almost hundred-fold reduction in the temperature across the specimen. Analysing the numerical values in Figure 7.9, we see that the temperature pulse width predicted by the C-V model equals the original heat pulse width $t_p = 0.005$. At the same time, the other models predict a temporal pulse broadening up to about $t = 2.5$. This conservation of the pulse width and the sharp wave fronts, is in accordance with the theory of the C-V model [OT94] [Tzo97]. In

contrast to the C-V model, the pulse shapes predicted by the other models skew to the right.

Although not typically of interest in thermorefectance, the large reduction in temperature across the specimen, prompts us to investigate the predicted temperature profiles in the interior of the specimen. Figure 7.10 shows the respective temperature profiles at $x = 0.2$. The maximum temperature values are approximately an order of magnitude higher than the values at $x = 1$. Calculating the temperature profiles at various x positions (results not shown here), shows that pulse width broadens with x (except for the C-V model), with a simultaneous decrease in pulse height. By comparing Figure 7.9 and Figure 7.10, we also notice that the pulse skewing increases with x .

Since the endpoint at $x = 1$ is insulated we expect that the thermal energy delivered at $x = 0$ by the pulsed source, will be conserved within the specimen, *i.e.* the area under the temporal profile will remain at a constant value. Following from our discussion in Section 6.9.1, the heat energy \mathcal{E} delivered to (and therefore transferred through) the specimen by a single laser pulse is given by $\mathcal{E} = \int_0^{t_p} P_{peak} dt$, where P_{peak} is the laser peak power. Since we model the heat pulse as a temperature step function, we can say that $\int_0^{\tau_p} T(0, t) dt$ (with $T(0, t)$ defined in Eq. (7.3.1)) represents the amount of heat transferred into the specimen. With $t_p = 0.005$ in the present numerical example, we have $\int_0^{\tau_p} T(0, t) dt = \int_0^{t_p} T(0, t) dt = 0.005$. For the temperature profiles in Figures 7.9 and 7.10, the areas under the profile from $t = 0$ to $t = \tau_p = 5$ are calculated using numerical integration. Two observations are made: firstly, for a given x position, the areas for the respective models are equal at ≈ 0.005 , and secondly, the area remains constant at a value of ≈ 0.005 , irrespective of the x position.

The modal analysis summary in Section 7.3.3 provides an explanation for the pulse broadening and skewing of the pulse profile in the case of the C-V and DPL-I models. For the C-V model, from Equations (7.3.22), (7.3.23) and (7.3.27) (with $\gamma_k = \gamma$) the contribution to the series solution for $u_1(x, t)$ by the k -th mode is given by

$$\frac{2}{\nu_k} e^{-\gamma t} \left(\cos \omega_k^d t + \frac{\gamma}{\omega_k^d} \sin \omega_k^d t \right) \sin \nu_k x. \quad (7.5.1)$$

We consider only the underdamped modes since propagation speeds are not associated with overdamped modes. A standard trigonometric identity shows that

$$\cos \omega_k^d t \sin \nu_k x = \frac{1}{2} \left(\sin(\nu_k x + \omega_k^d t) + \sin(\nu_k x - \omega_k^d t) \right). \quad (7.5.2)$$

7.5. THERMOREFLECTANCE CASE STUDY: LOW DUTY RATIO r_d 155

From standard wave theory, the function $\sin(\nu_k x - \omega_k^d t)$ represents a wave that is propagating to the right at a speed ω_k^d/ν_k and $\sin(\nu_k x + \omega_k^d t)$ a wave propagating to the left at the same speed. The product $\sin \omega_k^d t \sin \nu_k x$ can be expressed in a similar way. Therefore, for each of the underdamped modes of the C-V model, the propagation speed associated with the k -th mode is given by

$$\frac{\omega_k^d}{\nu_k} = c \sqrt{1 - \frac{\gamma^2}{c^2 \nu_k^2}} = c \sqrt{1 - \frac{1}{4\alpha\tau_q \nu_k^2}} < c, \quad (7.5.3)$$

and

$$\frac{\omega_k^d}{\nu_k} \rightarrow c = \sqrt{\alpha/\tau_q} \text{ when } k \rightarrow \infty. \quad (7.5.4)$$

As the limit is approached from below, the wave front speed for the C-V model is given by $c = \sqrt{\alpha/\tau_q}$ as stated by [TZ98] and others. For the current parameter values only the first mode of the C-V model is overdamped, and the propagation speeds associated with the underdamped modes quickly approach c . Hardly any pulse broadening occurs as the individual contributions to the series solution from the underdamped modes are propagated at almost the same speed. All the underdamped modes are damped by the same factor $e^{-\gamma t}$ and the shape of the temperature pulse is also retained, but with a reduction in the height of the pulse.

For the DPL-I model the propagation speeds for the underdamped modes are given by

$$\frac{\omega_k^d}{\nu_k} = c \sqrt{1 - \frac{\gamma_k^2}{c^2 \nu_k^2}}. \quad (7.5.5)$$

In contrast to the C-V model, these propagation speeds for the underdamped modes differ widely and significant pulse broadening and changes to the shape of the pulse occur. Also keep in mind that for the DPL-I model the majority of the modes are overdamped, and for these modes no associated propagation speeds are available.

In the case of the Fourier model, where we have an infinite propagation speed for the thermal disturbance, a change in temperature at $x = 0$ is experienced simultaneously throughout the specimen. Initially the heat energy is concentrated close to the surface region, whereafter the energy is gradually distributed throughout the specimen, resulting in a broad temperature pulse that decreases with x . For the DPL-II model all the modes are overdamped, and there are no finite propagation speeds associated with the individual modal contributions to the series solution. This suggests that the pulse

broadening that occur for the DPL-II model can be explained in the same way as for the Fourier model.

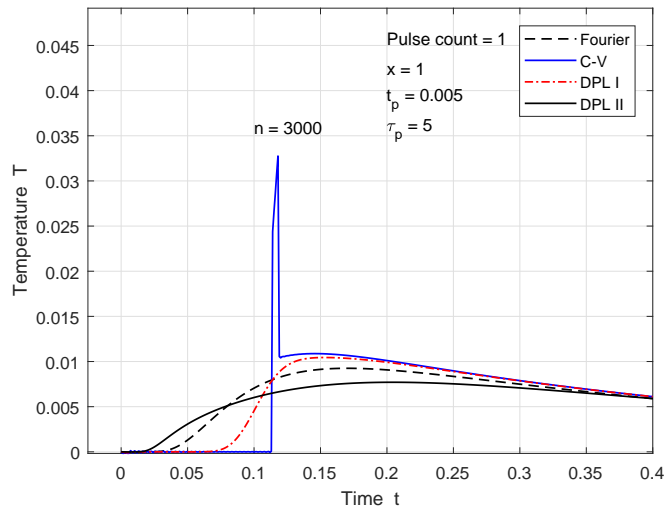


Figure 7.9: Temperature T at $x = 1$ displaying only the first pulse.
 $\tau_q = 0.012665$; $\tau_T^I = 0.002868$ ($\delta^I = 0.2265$); $\tau_T^{II} = 0.037995$ ($\delta^{II} = 3$)

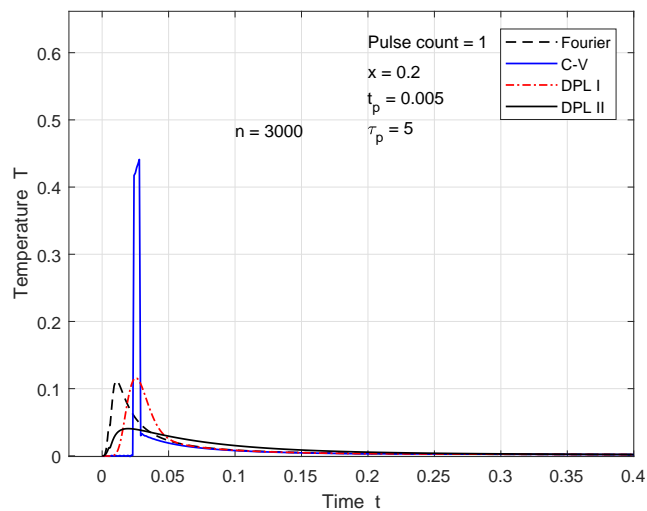


Figure 7.10: Temperature T at $x = 0.2$ displaying only the first pulse.
 $\tau_q = 0.012665$; $\tau_T^I = 0.002868$ ($\delta^I = 0.2265$); $\tau_T^{II} = 0.037995$ ($\delta^{II} = 3$)

It is well known that the C-V model predicts that when a heat pulse is incident at one boundary of a specimen, the wave front is reflected off the

7.5. THERMOREFLECTANCE CASE STUDY: LOW DUTY RATIO r_d 157

opposite boundary ([CT82] [LC04] [OT94]). Since the DPL-I model, with $\tau_T \ll 1$, approaches the C-V model, we choose to examine both models to see if we can find evidence of wave front reflection – the Fourier model is included as a reference. Firstly, both the C-V and the DPL-I model predict reflected pulses. In Figure 7.11 the peak values of the reflected pulses at $x = 0.8$ are lower than that of the incoming pulses. At a fixed position closer to $x = 1$, the reflected pulses have higher peak values. In Figure 7.12, at $x = 1$, only one temperature pulse appears which is the superposition of the incoming and reflected pulses.

Secondly, the DPL-I model shows the same behaviour as the C-V model, with respect to its predicted pulse width. The pulse width remains constant and the peak height decreases with x . The reflected pulse widths of both models are the same as the incoming pulses. The peak heights for the DPL-I model are approximately equal to the heights of the sharp thermal wave fronts of the C-V model at $x = 0.8$ when they arrive at this position. The areas under the temperature profiles are calculated for $x = 0.2$, $x = 0.8$ and $x = 1$ (note that $\tau_T^I \ll 1$ for the DPL-I model in this case) and are found to remain at the same value of ≈ 0.005 as the areas determined for Figures 7.9 and 7.10. The area is again conserved, even though there is hardly any broadening of the pulse widths and the pulse shapes are retained. Noticeable reflected pulses are present and these contribute to the calculated area.

It is interesting to see that the wave front arrival times correspond to the times predicted by the theory. As discussed earlier, the dimensionless speed of the wave front is given by $c = \sqrt{\alpha/\tau_q}$. Using this equation, the predicted arrival time of the wave front at $x = 0.8$ is $t = 0.0903$, which corresponds well with the wave front arrival time in Figure 7.11 ($t = 0.092$). A similar calculation, assuming that the wave front has traveled a dimensionless distance of 1.2, shows that the reflected wave front is expected to arrive back at $x = 0.8$ at $t = 0.135$. Again this corresponds well with the value observed in Figure 7.11.

7.5.2 Effect of lag time ratios δ

In the following numerical experiments, we investigate how the value of δ influences the differences and similarities between the DPL, C-V and Fourier model predictions. Referring to Section 6.8, the range of possible values for δ is: $0 < \delta^I < 1$ and $\delta^{II} \geq 1$.

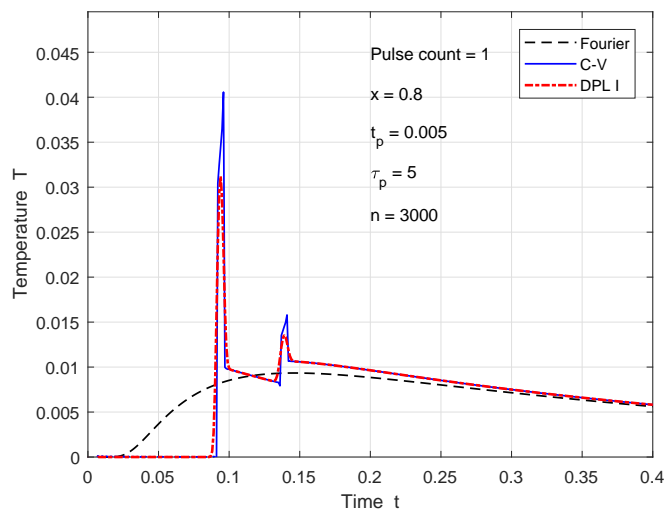


Figure 7.11: Temperature T at $x = 0.8$ displaying only the first pulse; including the C-V model.

$$\tau_q = 0.012665; \tau_T^I = 0.000025 \quad (\delta^I = 0.001974)$$

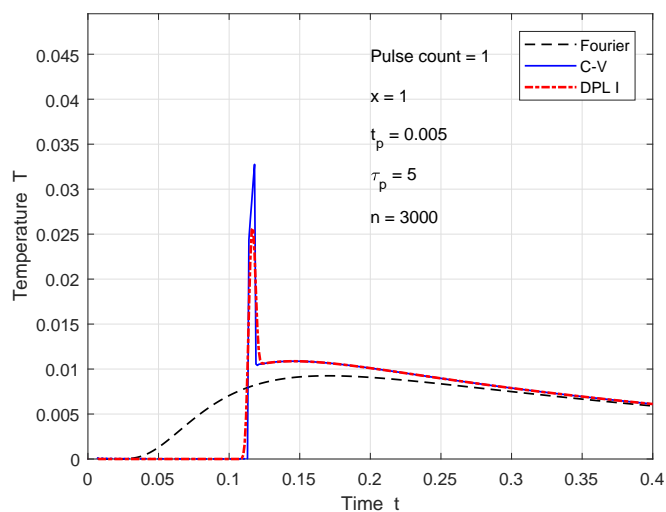


Figure 7.12: Temperature T at $x = 1$ displaying only the first pulse; including the C-V model.

$$\tau_q = 0.012665; \tau_T^I = 0.000025 \quad (\delta^I = 0.001974)$$

Case $\delta^I \rightarrow 0$:

In the first experiment we investigate what happens when $\delta^I \rightarrow 0$. We do this

7.5. THERMOREFLECTANCE CASE STUDY: LOW DUTY RATIO $r_d 159$

by either reducing τ_T^I and keeping τ_q fixed at the reference value, or increasing τ_q and keeping τ_T^I fixed at the reference value. The former case is already discussed in Section 7.5.1 (Figures 7.11 and 7.12). For $\tau_T^I = 0.000025$ (or $\delta^I = 0.001974$) the DPL-I temperature profiles at $x = 0.8$ and $x = 1$, have narrow smooth pulses with the pulse width equal to that of the C-V profile. This resemblance is expected as $\tau_T^I \ll 1$.

Increasing τ_q by a factor 4 to 0.05066 whilst keeping $\tau_T^I = 0.002868$, we have $\delta^I = 0.0566$. We compare the DPL-I profile with the Fourier profile (looking at the insert in Figure 7.13), and at the same compare this result with Figure 7.10, where $\delta^I = 0.2265$. In Figure 7.10 the Fourier and DPL-I temperature peaks are almost the same and the DPL-I profile starts to increase shortly after the Fourier profile. In the case of Figure 7.13 the DPL-I temperature peak is more than double the Fourier peak, and the delay before the temperature increase starts, is longer. With Figures 12 and 13 showing that the DPL-I model (with $\delta^I = 0.001974$) approaches the C-V model, the indication is that the DPL-I model in this case, with $\delta^I = 0.0566$, is approaching the C-V model. This suggests that the DPL-I model shows C-V behaviour not only when $\tau_T^I \ll 1$ but also when $\delta^I \ll 1$ ($\delta^I \rightarrow 0$).

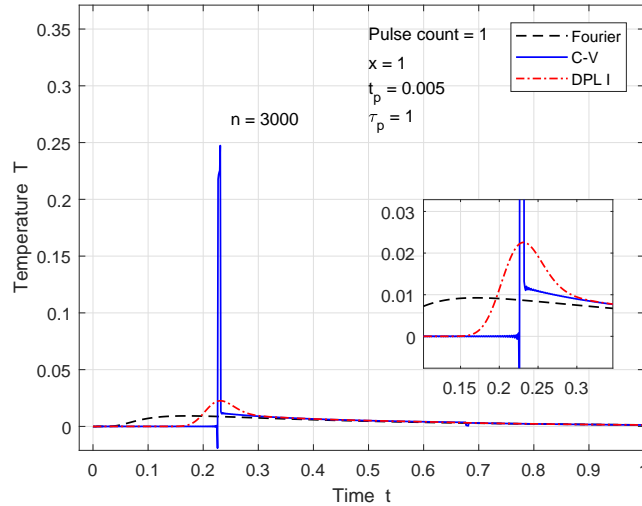


Figure 7.13: Temperature T at $x = 1$, displaying only the first pulse. $\tau_q = 0.05066$; $\tau_T^I = 0.002868$ ($\delta^I = 0.0566$)

Case $\delta^I \rightarrow 1$:

The second experiment investigates the case when $\delta^I \rightarrow 1$. We first use $\tau_T^I = 0.002868$ and decrease τ_q by a factor of 4 to 0.00316625 (Figure 7.14 – profile ‘DPL I’), and then fix τ_q at the reference value of 0.012665 and increase τ_T^I by a factor of 4 to 0.011472 (Figure 7.14 – profile ‘DPL I a’). We find that $\delta^I = 0.906$. In the ‘DPL I’ case, the DPL-I temperature profile coincides almost perfectly with the Fourier profile. This is ascribed to the fact that the lag times are relatively small (almost negligible), ensuring an almost perfect match between the DPL-I and Fourier models. Due to the substantially longer lag times, compared to the ‘DPL I’ case, the ‘DPL I a’ temperature profile is shifted slightly to the right of the Fourier profile, even though δ^I is the same for both ‘DPL I’ and ‘DPI I a’ cases.

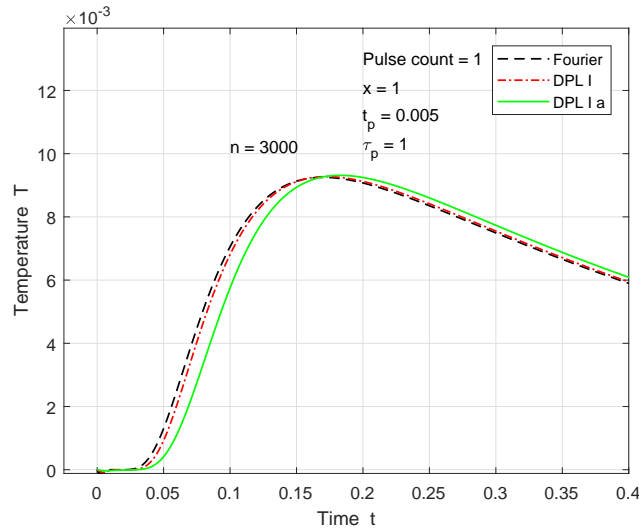


Figure 7.14: Temperature T at $x = 1$, displaying only the first pulse. $\tau_q = 0.00316625$; $\tau_T^I = 0.002868$ ($\delta^I = 0.906$)

Case $\delta^{II} = 1$:

The third experiment’s aim is to study how the DPL-II model predictions compare with the Fourier model. We start by decreasing τ_T^{II} to 0.012665, with τ_q fixed at the reference value, (*i.e.* $\delta^{II} = 1$). The result is that the DPL-II temperature profile closely follows the Fourier profile, although lagging slightly behind the Fourier profile (Figure 7.15 – profile ‘DPL II’). This result is in agreement with Tzou’s prediction that the Fourier and DPL models correspond when $\delta^{II} = 1$ (see Section 2.5.2). Next, we increase τ_q to 0.037995, with τ_T^{II} fixed at the reference value, (*i.e.* $\delta^{II} = 1$). The result is

7.5. THERMOREFLECTANCE CASE STUDY: LOW DUTY RATIO r_d 161

that the lag between the DPL-II temperature profile and the Fourier profile increases, with the peak temperature also reducing (Figure 7.15 – profile ‘DPL II a’).

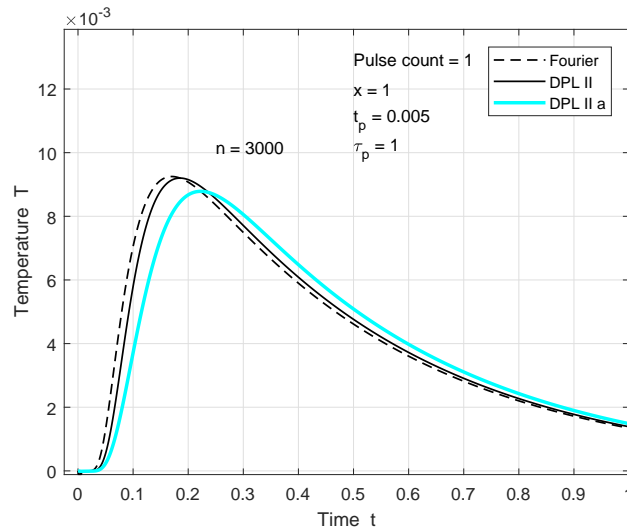


Figure 7.15: Temperature T at $x = 1$ displaying only the first pulse. $\delta^{II} = 1$

Case $\delta^{II} > 1$:

We already have an example of the effect when $\delta^{II} > 1$ (Figure 7.9 illustrates the case where $\delta^{II} = 3$). We explore here what happens if we increase δ^{II} even further. We start by increasing τ_T^{II} by a factor of 2 to 0.07599, with τ_q fixed at the reference value, (*i.e.* $\delta^{II} = 6$). The DPL-II temperature peak is considerably lower than the Fourier model’s peak and the temperature rise starts earlier (Figure 7.16 – plot ‘DPL II’). Decreasing τ_q by a factor of 2 to 0.0063325, with τ_T^{II} fixed at the reference value, (*i.e.* $\delta^{II} = 6$), we find that the peak temperature value increases, although still lower than the Fourier peak temperature (Figure 7.16 – plot ‘DPL II a’).

In summary, we conclude that if δ^I is close to 0, the DPL-I model shows a sharp thermal wave front similar to the C-V model. If δ^I is close to 1, then the DPL-I model predictions are close to the Fourier model, although the relative magnitudes of the lag times should also be considered. Similarly, if δ^{II} is close to 1, then the DPL-II model predictions are close to the Fourier model. In general, we see that if $\delta < 1$, the temperature rise starts later and the lower the δ value is, the higher the peak temperature values. In contrast, if $\delta > 1$, the temperature rise starts at an earlier stage and the higher the δ

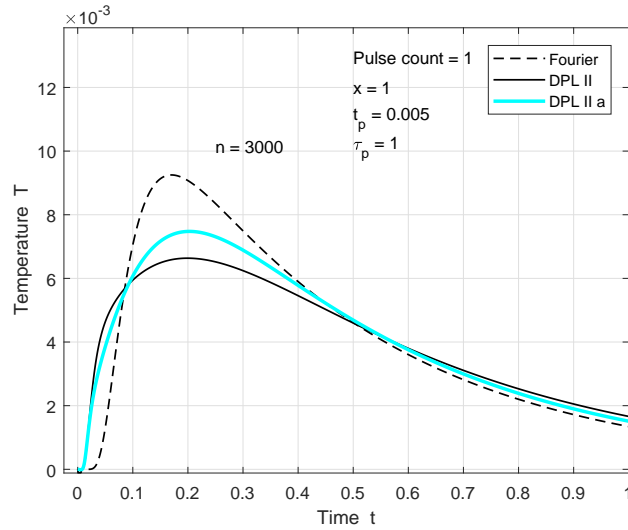


Figure 7.16: Temperature T at $x = 1$ displaying only the first pulse. $\delta^{II} = 6$

value, the lower the predicted temperature peak values become. In all cases the DPL, C-V and Fourier models predict the same temperature values, after a sufficiently long time.

7.6 Bio-heating case study: high duty ratio r_d

In this section we use experimental and specimen parameters applicable to bio-heating [MYSY21]. The example is a blood specimen, with thickness $d = 2$ mm and thermal diffusivity $\alpha = 5.881 \times 10^{-8} \text{ m}^2\text{s}^{-1}$. With no preference for either the diffusion time t_d or the half-time $t_{1/2}$ found in literature, we choose the half-time $t_{1/2}$ to be the scaling parameter, since we prefer a scaling factor closest to the typical pulse widths used in our numerical experiments ([BTY11] [PJBA61]). Then $t_0 = 0.1388d^2/\alpha \approx 10$ s. A typical heating pulse width is $t_p = 0.5$ s and the duty ratio $r_d = 0.5$, implying that $\tau_p = 1$ s.

The dimensionless pulse width and pulse period are $t_p = 0.05$ and $\tau_p = 0.1$ respectively, and the dimensionless thermal diffusivity is $\alpha = 0.1388$. Our first aim is to find lag times that, during an initial time interval, yield distinct differences between the temperature profiles predicted by the respective models. Again, this is done following the guidelines in Sections 6.3 and 6.7 on how to determine appropriate lag times. We find $\tau_q = 0.024333$,

$\tau_T^I = 0.017395$ and $\tau_T^{II} = 0.072999$. The lag time ratios are $\delta^I = 0.72$ and $\delta^{II} = 3.0$.

In bio-heat applications one is generally interested in the temperature at the incident surface as well as in the interior of the specimen. We also notice that the duty ratio in this case has roughly the same magnitude as that used in Section 7.4. An investigation of the temporal profiles will therefore lead to the same results as in Section 7.4, *i.e.* the C-V model is characterised by a sharp wave front; the instants at which the temperature starts to rise, as predicted by the different models, follow the same sequence (Fourier first, then DPL-II, DPL-I and lastly C-V); the peak temperature increases with each consecutive pulse; and the peak temperatures predicted by each model, differs.

As an example, In Figure 7.17, we show the temporal temperature profiles at $x = 0.5$ for a 7-pulse case. Except for the C-V model, almost complete merging of the individual pulses have occurred. On the insert the 7 wave fronts for the C-V model are visible. The DPL-II model predicts the lowest temperature, the DPL-I and Fourier, an equal and slightly higher temperature, with the C-V model the highest temperature. Apart from the slight peak difference, the models predict the same profile over the time span of the merged pulse. When compared to the temperature profiles in Figure 7.3, in this case the merging of pulses resulting from pulse broadening is more advanced.

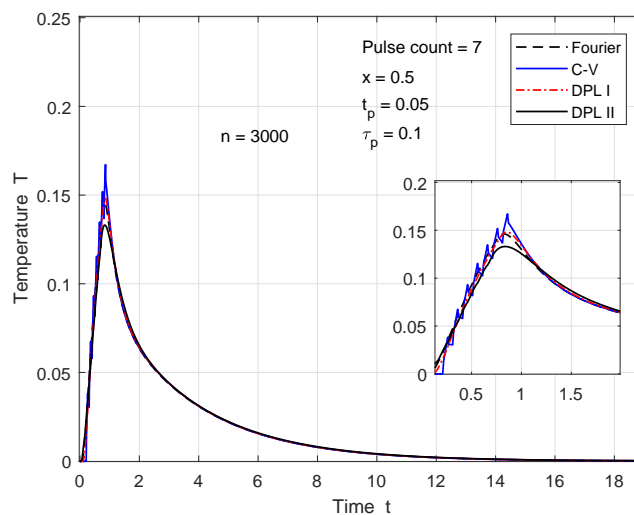


Figure 7.17: Temperature T at $x = 0.5$ for a 7-pulse problem

We also know from Section 7.4 that the temperature reaches a plateau level after a sufficient number of pulses, and that the pulses merge at some point in the interior of the specimen. These observations follow from the temporal profiles at fixed x points in Section 7.4. We now turn to spatial temperature distributions at fixed times t .

We ascribe the temperature increase per pulse to the fact that, due to the high duty ratio ($r_d = 0.075/0.15 = 0.5$), the temperature at a given x position does not return to its original zero level before the next pulse is incident at $x = 0$. This suggests that on the spatial temperature profiles more than one pulse will be visible at a fixed time t . In Figure 7.18 we use a three-pulse example, with $t_p = 0.05$ and $\tau_p = 0.1$, to evaluate the spatial temperature distribution at $t_{ev} = 0.199$ (t_{ev} indicates the evaluation time), just before the third pulse starts (*i.e.* during a "pulse OFF" event). We immediately notice that all the models, except the C-V model, predict single, merged pulses. The C-V model predicts two separate pulses, indicated by the sharp wave fronts. For the DPL-I and DPL-II temperature distributions the sharp rises close to $x = 0$ is noticeable. This is due to the delays τ_T^I and τ_T^{II} in forming temperature gradients. As $\tau_T^I < \tau_T^{II}$ the DPL-I model has a shorter delay and more quickly adjusts to the zero temperature at $x = 0$ after the start of the "pulse OFF" event. Ignoring the C-V profile's wave front, the models agree from about $x = 0.4$ onwards.

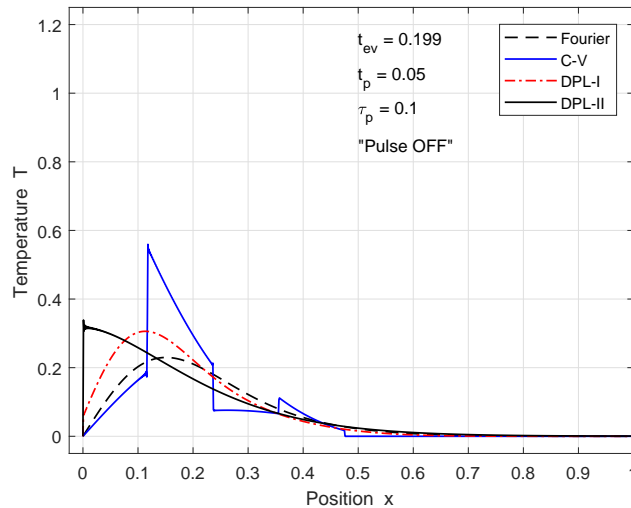


Figure 7.18: Spatial temperature distribution at $t_{ev} = 0.199$

At $t_{ev} = 0.205$ ("pulse ON" event) we see how the third pulse deposits heat energy into the specimen close to $x = 0$ (Figure 7.19). The temperature

disturbance due to the first two pulses are present as a single merged peak for both the Fourier and DPL-I model, whilst the DPL-II temperature profile smoothly decreases from $x = 0$ to the interior of the specimen. The C-V model maintains distinct wave fronts, and Gibbs oscillations occur near $x = 0$.

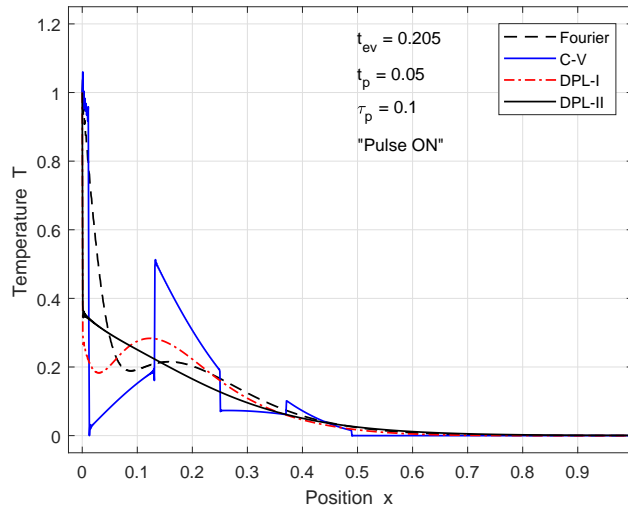


Figure 7.19: Spatial temperature distribution at $t_{ev} = 0.205$

We next investigate the effect of a large number of pulses on the spatial distribution of the temperature in the specimen. We study a 50-pulse example, using the same pulse parameters and lag times as for Figure 7.18. Figure 7.20 gives the result just before the 50th pulse starts, and Figure 7.21 just after. Increasing the number of pulses leads to a more uniform temperature distribution throughout the specimen, except for the region up to $x \approx 0.3$ where the different models predict different distributions.

We are also interested in the effect of reducing the duty ratio r_d . We reduce r_d by either reducing the pulse width t_p whilst maintaining the pulse period at $\tau_p = 0.1$, or maintaining t_p whilst increasing τ_p . We first reduce the duty ratio from $r_d = 0.5$ by a factor of 2 to 0.25, by choosing $t_p = 0.025$ and $\tau_p = 0.1$. We see that the temperature level in the second half of the specimen reduces by the same factor of 2 from $T \approx 0.4$ (Figure 7.22) to $T \approx 0.2$ (Figure 7.23). In Figure 7.24 we maintain $t_p = 0.05$ and increase τ_p by a factor of 2 to 0.2, with r_d remaining at 0.25. The temperature level in the second half of the specimen increases to $T \approx 0.24$. On the C-V profile only one wave front is visible as opposed to the two wave fronts in Figure 7.23. From these results we deduce that there does not

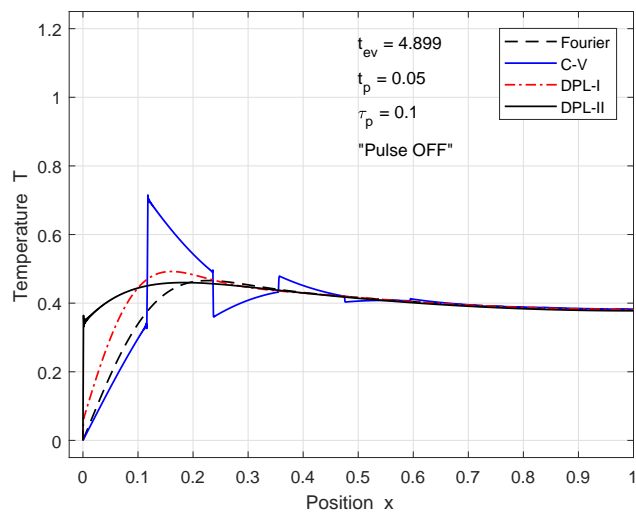


Figure 7.20: Spatial temperature distribution at $t = 4.899$; before pulse 50 starts; $r_d = 0.5$.

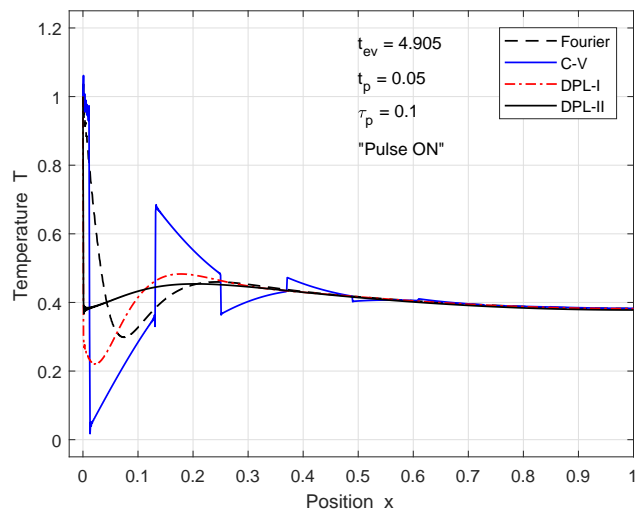


Figure 7.21: Spatial temperature distribution at $t = 4.905$; after pulse 50 starts; $r_d = 0.5$.

necessarily exist a direct relation between the factor by which the duty ratio r_d is reduced and the corresponding reduction in the temperature level. The two examples we give here, has the same duty ratio, but the pulse width t_p differs, resulting in different temperature levels.

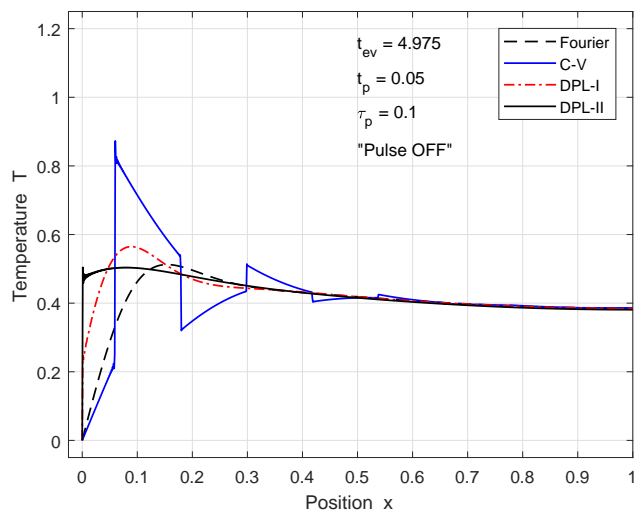


Figure 7.22: Spatial temperature distribution at $t = 4.975$, after pulse 50 stops; $r_d = 0.5$.

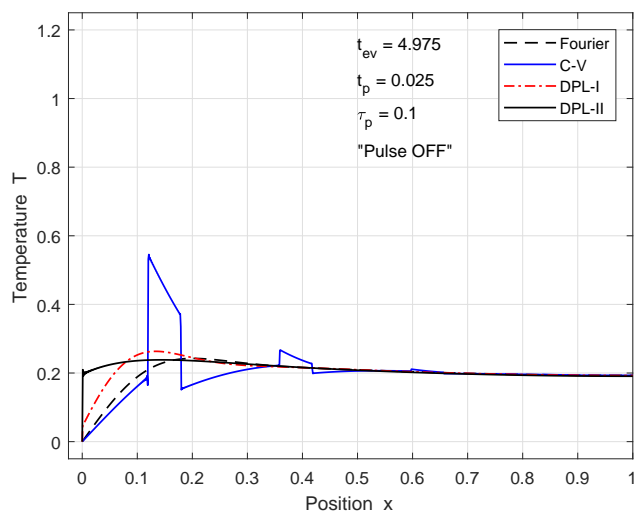


Figure 7.23: Spatial temperature distribution at $t = 4.975$; $r_d = 0.25$.

7.7 Conclusion

Heat transfer behaviour in a specimen subject to multiple heat pulses is investigated, for the Fourier, Cattaneo-Vernotte and dual phase lag models respectively. One dimensional models are used, and as is commonly done,

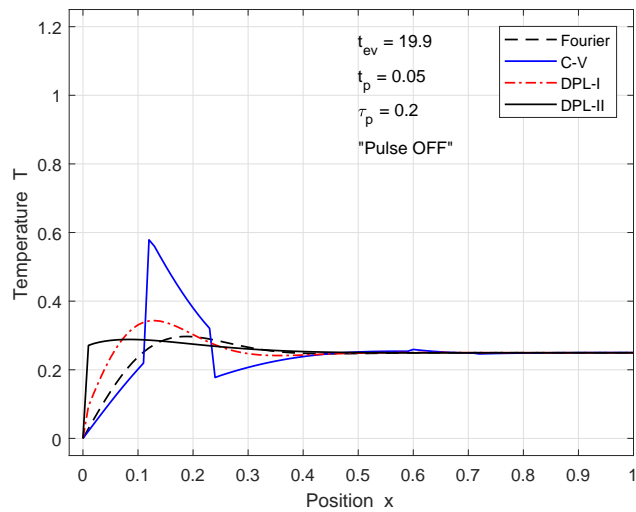


Figure 7.24: Spatial temperature distribution at $t = 9.95$; τ_p increased; $r_d = 0.25$.

the effect of the heat pulses is modelled as a temperature step function at the one endpoint. To solve the multi-pulse problem, a series of single-pulse problems is considered where the final temperature distribution for a given pulse cycle, provides the initial temperature for the subsequent pulse cycle. We successfully adapt the separation of variables procedure in Section 6.9 for calculating the modal series solution for a single-pulse problem to solve the multi-pulse problem. In addition, the solution for the multi-pulse problem is expressed in terms of the solution of a homogenised problem associated with the single-pulse problem. Using the truncated modal series as an approximate solution proved to be an effective method for a numerical investigation into the properties of the solutions of multi-pulse problems. Both temporal temperature profiles (temperature versus time at a fixed position) and spatial profiles (temperature versus position at a fixed time) are readily available.

The aim of the numerical experiments is two-fold: to compare the temperature predictions by the Fourier, C-V and DPL models, and to identify situations where the C-V and DPL temperature profiles differ significantly from those of the Fourier model. The numerical simulations cover a wide range of physical parameters. Two experimental techniques where pulsed heating is used, thermorefectance and bio-heating, provide realistic physical parameters for the heat pulses. These values are used for designing numerical experiments that cover a wide range of physical scenarios. Values for the phase lags in the C-V and DPL models are harder to find, and we use

the upper bounds given in Section 7.3.4 as guidelines. These upper bounds ensure that the temperature predictions for the C-V and DPL models approach those of the Fourier model after some time, as in many heat transfer situations the Fourier model provides acceptable results after a sufficiently long time.

As a first step, the parameter values are chosen as for the single-pulse problem in Section 6.10, and the temperature profiles are compared with the multi-pulse case. There are obvious similarities between the single-pulse and multi-pulse cases, but we observe two interesting phenomena for the multi-pulse case, namely the merging of temperature pulses when observed at fixed points deeper into the specimen, and when increasing the duty ratio, and/or the number of pulses, a plateau value is established in the specimen for the peak temperatures.

For simulations associated with thermoreflectance experiments we use the diffusion time t_d as the time scaling factor, as this is a well-known concept in the field. In this case the duty ratio of the laser pulses is low and the temporal temperature profiles at the insulated endpoint of the specimen is of main interest. Key findings for these simulations are that distinct pulses persist in the temperature profiles throughout the specimen, even though a broadening of the pulses occur towards the insulated endpoint. Reflected temperature waves are observed in some of the temperature profiles of the C-V model, as well as in some of those of the DPL model.

For bio-heat applications the duty ratio is high and the spatial temperature profiles are of interest. In this case we use the half-time $t_{1/2}$ as the time scaling factor. Key findings for these simulations are the noticeable merging of pulses, leading to a uniform spatial temperature distribution, as well as the clear effect of the time lag in the temperature gradient at the onset and termination of each pulse. Although numerical calculations were performed for example problems including up to 50 pulses, the computational time never exceeded one minute.

The truncated modal series solution proved to be an efficient procedure for investigating the properties of the multi-pulse heat transfer problems, and modal properties provide insight into the behaviour of the solutions.

Chapter 8

Conclusion and future research

8.1 Overview

The aim of our research was to study heat transfer in specimens subject to short-pulse heating. Literature studies showed that other models are proposed as alternatives to the Fourier model, which is considered to be inadequate in predicting the temperature in certain cases ([TZ98]). Our main interest is in the C-V ([OT94]) and DPL ([Tzo95a]) models, frequently suggested as alternatives to the Fourier model. We observed two interesting aspects during our literature study: the occurrence of unwanted or spurious oscillations when approximating the C-V model using numerical techniques; and the lack of reliable values for the lag times τ , τ_q and τ_T that appear in the C-V and DPL models. We therefore focused our efforts on the comparison of the Fourier, C-V and DPL models, and determining the origin of the unwanted oscillations, with the intention of proposing a solution.

In Chapter 2 the derivation of the model equations is presented, including a summary of the characteristics of the Fourier, C-V and DPL models. The discussion of the DPL model is preceded by a section on the microscopic effects of heat transfer in metals and the derivation of the two-step heat transfer model, from which the DPL model follows. We discussed the heat absorption process in a specimen as it determined how we formulated the boundary conditions in our model problems. We derived the dimensionless versions of the heat conduction models, together with the boundary and initial conditions on which this study was based.

The issue of unwanted oscillations, related to the CT-benchmark problem (a special case of the C-V model), was investigated in Chapter 3. This problem

was originally formulated by Carey and Tsai in 1982 [CT82]. It was shown that the unwanted oscillations is the result of an ill-posed problem and not due to the choice of the numerical technique used to solve the problem. The CT-benchmark problem was re-formulated to a problem that has a smooth initial condition. The problem was divided into three auxiliary problems. D'Alembert's method was used to obtain exact solutions for the first two auxiliary problems, and the finite element method was used to obtain an approximate solution to the third auxiliary problem. A numerical algorithm was developed, resulting in a solution method that can successfully track the sharp wave front but without a discontinuity, *i.e.* free of oscillations.

In Chapter 4 we started off by introducing model problems for mechanical vibrations. The similarities with the hyperbolic-type heat conduction problems (*i.e.* the C-V and DPL models) were pointed out, and the terminology, *e.g.* overdamped and underdamped modes, were adopted for use with the heat conduction problems. General abstract formulations were developed for the Fourier, C-V and DPL models. Following this, variational forms were derived and expressed in terms of defined bilinear forms. Ultimately, weak variational forms of these models were derived to apply existence theory to the C-V and DPL models.

In Chapter 5 we applied the modal analysis method to the general second order hyperbolic equation expressed in variational form. Substitution of a trial solution into this abstract equation led to an eigenvalue problem. With the requirement that the eigenvectors form an orthogonal sequence, a formal series solution was derived. In order to apply the model formulations derived in Chapter 4 to subsequent chapters, the formulations were adapted to include the physical parameters that appear in the heat conduction models. The convergence of the series solution was expressed in terms of the energy norm $\|\cdot\|_V$ and inertia norm $\|\cdot\|_W$. It was found that the partial sum $u_N(t)$ converges to the solution $u(t)$ in the energy norm and $u'_N(t)$ to the derivative $u'(t)$ in the inertia norm, for all $t > 0$. Therefore, the accuracy of these approximations relies on the accuracy of the partial sum approximations at time $t = 0$.

Chapter 6 is devoted to a comparison between the Fourier, C-V and DPL heat conduction models. Two important aspects had to be dealt with before starting with the comparison: deciding on the initial value for the numerical experiments, and determining realistic values for the lag times used in the numerical experiments.

Series solutions were derived for the model problems based on the C-V, DPL and Fourier models in Section 6.2. We proposed a smooth temperature distri-

bution function to approximate the initial value. It is however not practical to calculate the Fourier coefficients for this initial value and we therefore opted to use the simpler, discontinuous initial condition. In order to ensure that the accuracy achieved when using this discontinuous initial value is acceptable, error estimates in the energy and inertia norms were calculated and used as a guideline to decide on the number of terms required in the series approximation.

To determine realistic lag times for our numerical experiments, we relied on the premise that, given a sufficiently long time has elapsed, the model predictions from the C-V and Fourier models will correspond. For $\tau_q \ll 1$, this means that for the first mode, the respective time dependent functions for the C-V model will be equal to that of the Fourier model after a sufficiently long time. To determine τ_T we further assumed that $\tau_T \ll 1$, ensuring that the DPL model approaches the Fourier model (refer to Section 6.7). We derived upper bounds for the lag times τ_q and τ_T , given by

$$\tau_q \leq \frac{\varepsilon}{\alpha\pi^2} \text{ and } \tau_T \leq \frac{4\varepsilon}{\alpha\pi^2},$$

with ε a user specified accuracy and α the dimensionless thermal diffusivity. The transformation of α to the dimensionless value is done using a reference time t_0 , which can be adjusted to represent the time scales characteristic of the physical scenario being investigated. Adjusting t_0 , scales α and consequently τ_q and τ_T to achieve a range of values for the lag times that are realistic for a given numerical experiment.

In Section 6.4 we introduced the concept of a *wane time* t_w as the time instant at which the wave front, characteristic of the C-V model, disappears. We predicted that the solutions for the Fourier and C-V models will be the same at the time that the wave front disappears. An expression was derived for the wane time, $t_w = -2\tau_q \ln(\sigma)$, where σ is equal to the ratio of the reduced wave front height at $t = t_w$, to the original height at $t = 0$.

The comparison between the Fourier, C-V and DPL models for the continuous heating model problem started off by testing our assumption that the respective model predictions will agree after a sufficiently long time has elapsed, *i.e.* at $t \approx t_w$. Additional numerical experiments were performed to study the respective contributions of the overdamped versus underdamped modes to the predicted temperature profiles, and especially how it affects the wave front present in the C-V model. The DPL-I model's dependency on the over- and underdamped modes to achieve accurate temperature predictions, was investigated. Also of interest was the behaviour of the DPL models close to $x = 0$, in view of the discontinuity that exists at $x = 0$.

The approach to solving the single-pulse model problem was to divide the problem into two sub-problems corresponding to the different boundary conditions at $x = 0$ (refer to Section 6.9.1). We referred to the sub-problems as “Problem 1” and “Problem 2” respectively. The solution derived for the continuous heating model problem was used to solve Problem 1, *i.e.* when the pulse is applied. To solve Problem 2 (when the pulse is stopped), the end temperature distribution for Problem 1 is assigned as the initial temperature distribution for Problem 2, continuing with the solution for Problem 1 to obtain the solution for Problem 2. The model comparison mainly focused on how each model behaves close to $x = 0$, how the peak temperatures compare, and how the heat pulse propagates into the specimen. Interesting observations were made regarding the resemblance between the DPL-I model and the C-V model when $\tau_T \ll 1$, and the behaviour of the respective models when the pulse is stopped.

In Chapter 7 we considered the multi-pulse model problem. It is similar to the single-pulse problem, except that the multiple of m identical heat pulses is modelled as a periodic step function consisting of m steps. The model problem was divided into $2 \times m$ sub-problems, where the end temperature distribution for a given sub-problem becomes the initial distribution for a subsequent sub-problem. The solution to the multi-pulse problem with m pulse cycles is given by a sequence of functions

$$T_n(x, t) = 1 - u_1(x, t - t_{n-1}) + T_{n-1}(x, t) \quad (t_{n-1} \leq t < t_n)$$

$$T_{n+1}(x, t) = T_n(x, t) + u_1(x, t - t_n) - 1 \quad (t_n \leq t < t_{n+1})$$

for $n = 1, 3, 5, \dots, 2m - 1$. This solution is made possible since continuity allows linking of the solutions of the sub-problems. The focus of the model comparison was to examine the effect of the duty ratio r_d and the number of pulses m on the predicted temperature profiles. Numerical experiments were performed using parameter values typical of thermorefectance and bio-heating applications.

8.2 Key results

It was shown that the unwanted oscillations related to the CT-benchmark problem, as formulated by Carey and Tsai in 1982, is the result of an ill-posed problem and not due to the choice of the numerical technique used to solve the problem. The CT-benchmark problem was re-formulated to have a smooth initial condition, and divided into auxiliary problems that were solved using D'Alembert's and the finite element method. The solution method is able to track the wavefront without a discontinuity, ensuring oscillation-free results.

The theory and terminology of vibration analysis were incorporated into the heat conduction models. Weak variational formulations of these models (in terms of bilinear forms) were presented and the well-posedness of the DPL and C-V model problems was established, based on a general existence result by Van Rensburg and Van der Merwe in 2002.

The modal analysis method was applied to the general second order hyperbolic equation and the formal series solution of the heat conduction problems were derived. Convergence of the series solution was proved in terms of the energy and inertia norms. An important conclusion was that the accuracy of the partial sum approximations of the series solutions, relies on the accuracy of the partial sum approximations at time $t = 0$.

The comparison between the Fourier, C-V and DPL heat conduction models started with the task of deciding on a suitable initial condition. The discontinuous initial condition was preferred above a smooth temperature distribution function since it simplifies the calculation of the Fourier coefficients. Expressions were derived for the energy and inertia norm errors and were used as a guideline to determine the number of terms required for the calculation of the partial sums of the series solutions. This ensured accurate approximations for the solutions of the model problems, even though the discontinuous initial condition was used.

In order to perform numerical experiments with realistic lag time values, upper bounds for the lag times τ_q and τ_T were derived using modal analysis. The derivation relied on the assumption that the solutions for the C-V and Fourier models will be the same after a sufficiently long time. The lag times can be scaled using the expressions for the upper bounds, to represent the physical scenario of interest.

We introduced the concept of a *wane time* t_w as the time instant at which the wave front disappears, and predicted that the Fourier and C-V models will correspond at $t = t_w$. The comparison based on the continuous heating model

problem, proved that t_w is a reliable way to quantify the time required for the Fourier model and the C-V and DPL models to correspond. Regarding the respective contributions from the overdamped and underdamped modes, it was found that it is essential to initially include the underdamped modes of the C-V model since these modes capture the wave front. The DPL-I model requires both over- and underdamped modes to achieve accurate temperature predictions. Numerical experimentation showed that the DPL-II model does not resolve the discontinuity at $x = 0$ caused by the discontinuous initial value.

The solution strategy for the single-pulse problem was to divide the problem into two sub-problems, and assign the end temperature distribution for the first sub-problem, as the initial temperature distribution for the second sub-problem. The solutions for the sub-problems, linking the solutions in the end. We highlight two interesting observations. If $\tau_T \ll 1$, the DPL-I model resembles the C-V model, predicting a prominent wavefront, but with a smooth profile. When the pulse is stopped, the Fourier model predicts a sudden drop in temperature, whilst the other models further increase in temperature before experiencing a sharp drop in the C-V model case, and a gradual drop in the DPL case.

The solution strategy for the multi-pulse problem was similar to the single-pulse problem in that the identical heat pulses were modelled as a sequence of sub-problems, with the solution expressed as a corresponding sequence of functions. With a low duty ratio r_d (*e.g.* in the thermorefectance application) we observed distinct temperature pulses in the temperature profiles throughout the specimen, although a broadening of the pulses occur towards the insulated endpoint at $x = 1$ for the Fourier and DPL models. In the case of the C-V model the pulse width remained constant. For a high duty ratio r_d (*e.g.* bio-heat application) the temperature pulses merge in the interior of the specimen, and increasing the number of pulses at the same time, result in a temperature plateau being established in the interior of the specimen.

In conclusion, modal analysis proved to be successful in determining reliable dimensionless values for the lag times τ_q and τ_T , and was effective for the numerical investigations into the properties of the solutions of our model problems.

8.3 Future research

8.3.1 Background

In Chapters 6 and 7 we compared the Fourier, C-V and DPL heat conduction models using simplified model problems as test cases. The simplifications involved restricting ourselves to one-dimensional versions of these models, and the assumption that all the heat is absorbed instantaneously at the boundary $x = 0$. Both simplifications are justified: one-dimensional models are accepted in the thermophysical metrology community when determining the thermal diffusivity α , and the heat absorption model is one that was regarded as sufficient by Tzou ([Tzo97]), and Baumeister and Hamill ([BH69]) to study the lagging and wave behaviour of the DPL and C-V models respectively. Our model problems, together with the use of modal analysis, proved to be effective in gaining insight into the characteristics of the heat conduction models. In addition we also determined reliable values for the lag times τ_q and τ_T using modal analysis.

In Chapter 2 we discussed instances where researchers criticised each others experimental methodologies and approach in analysing the measurement results ([OA12]). In some cases researchers performed similar experiments, with some claiming they observed hyperbolic effects, whilst others claimed that the Fourier model is valid. Maillet ([Mai19]) also stated that proper experimental design is essential when comparing models and attempting to derive heat transfer parameters from the results.

Our suggestions for future research are aimed at addressing two aspects in heat transfer research:

1. Formulating realistic model problems that resemble properly designed measurement setups, thereby facilitating comparison with reliable experimental techniques.
2. Identifying suitable mathematical techniques to solve these model problems. In addition this requires that reliable values for model parameters (*e.g* lag times) are determined, and that model problems are well-posed and convergence of solutions proved.

In our opinion the experimental methodology applied by the thermophysical metrology community can be regarded as *state-of-the-art* with respect to the measurement of thermophysical parameters and have the potential to serve as a reliable validation of theoretical model predictions. We motivate

this as follows: the thermal diffusivity α is an important heat transfer parameter used in engineering applications, and having accurately measured values is therefore important. The expectation of scientists and engineers using thermophysical properties (*e.g.* α) in thermal modelling and design, is that these are reliably known and traceable to the International System of Units (SI), published by the *Bureau International des Poids et Mesures* (BIPM). The responsibility of coordinating international efforts to ensure reliable measurements of thermophysical properties of materials is assigned to the various working groups within the Consultative Committee for Thermometry (CCT), operating within the BIPM ([Bab10]).

We briefly introduced the two *standardized* methods used to measure α in Section 7.2: the laser flash method for measuring α in bulk specimens, and the thermoreflectance methods (also known as the ultrafast laser flash methods) used to measure α in thin film type specimens ([BTY11]). Both techniques rely on heat transfer modeling to calculate the value of α from the measurement results. The laser flash method relies solely on the one-dimensional Fourier (diffusion) model to analyse the measurement data ([AHZCB13]). In the case of the thermoreflectance methods, the metrology community has been relying on the Fourier model for the data analysis for quite some time, but experimental evidence exists that shows that the Fourier model is not adequate in describing the heat transfer behaviour for the *femtosecond* thermoreflectance method ([BFI62] [Bro90] [NTYB11]).

Thermoreflectance has the potential to exhibit both Fourier and non-Fourier heat transfer behaviour and we therefore suggest that model problems should be based on the technique of thermoreflectance, as developed and approved by the thermophysical metrology community.

8.3.2 Research suggestions

We suggest a two-fold approach to formulate realistic model problems. Firstly, an accurate source model should be formulated, *e.g.* the laser pulse's temporal characteristics, as well as the spatial absorption by the specimen have to be described by this model. Secondly, alternatives to the linearized DPL heat conduction model should be considered. Motivation for alternative heat conduction models can be found with the attempts to explain the results obtained during femtosecond thermoreflectance measurements. Nakamura *et al* ([NTYB11]) reports that their experimental results during approximately the first 2 picoseconds are not explained by the Fourier model. They studied the model predictions from two other models, namely the two-temperature

model and the *non-thermal* model and the conclusion was that the non-thermal model best explained the results during the first 2 picoseconds. The non-thermal model takes into account ballistic transport effects, *i.e.* implying longer electron-thermalization times, up to approximately 700ps ([HMWM97] [Sin10] [SVAIF94]) – see Section 2.4.1. Therefore the electron-thermalization time can be longer than the laser pulse width. Using a source model that assumes instantaneous heat absorption is therefore not going to track the ballistic phase of the electrons, the laser’s temporal behaviour, and the transition to a diffusive heat transfer condition.

Suggestions for alternative heat conduction models include, but are not limited to:

- Linearized DPL with source term
- Two-temperature model (TTM) – also known as parabolic-two-step model (PTS); with source term
- Hyperbolic-two-step model (HTS) – with source term
- Second-order DPL model – with source term

The choice of mathematical technique used to solve any of these models will be determined by the model equation itself as well as the requirement to prove convergence. At the same time it would be required that the models are well-posed. The requirement to determine reliable values for model parameters, remains.

We present an example model of a realistic source term $S(x, t)$ whereafter example model formulations, based on the above mentioned heat conduction models, will follow.

Source term $S(x, t)$

A model that describes both the temporal nature of a laser pulse, as well as the absorption profile in the specimen would be required. A typical laser pulse source $S(x, t)$ is modelled as follows ([QT93a] [TM94] [Tzo97])

$$S(x, t) = 0.94 \left(\frac{1 - R}{t_p \delta} \right) \exp \left[\left(-\frac{x}{\delta} \right) - 2.77 \left(\frac{t}{t_p} \right)^2 \right], \quad (8.3.1)$$

where R is the optical reflectivity, t_p is the laser pulse width and δ is the optical penetration depth of the laser.

To derive a specific model problem, $S(x, t)$ is included in the energy conservation equation

$$\rho c_p \partial_t T = -\partial_x q + S. \quad (8.3.2)$$

As shown in Chapter 2, the energy conservation equation is combined with the relevant constitutive equation. As an example we choose the linearized DPL constitutive equation,

$$q + \tau_q \partial_t q = -k \partial_x T + k \tau_T \partial_t (\partial_x T), \quad (8.3.3)$$

and arrive at the linearized DPL model equation, including a source

$$\partial_t^2 T + 2\gamma \partial_t T = c^2 \partial_x^2 T + c^2 \tau_T \partial_t \partial_x^2 T + \frac{c^2}{k} S + \frac{c^2}{k} \tau_q \partial_t S. \quad (8.3.4)$$

Linearized DPL model with source term

The dimensionless single-pulse model problem with a source term is given by

$$\begin{aligned} \partial_t^2 T + 2\gamma \partial_t T &= c^2 \partial_x^2 T + \tau_T c^2 \partial_t \partial_x^2 T + 2\gamma S + \partial_t S & (8.3.5) \\ \partial_x T(0, t) &= 0 \\ \partial_x T(d, t) &= 0 \\ T(x, 0) &= T_0 \\ \partial_t T(x, 0) &= 0. \end{aligned}$$

The initial condition $T(x, 0) = T_0$ assumes that heating starts from a stationary state. Since the typical heating period is very short it is assumed that the heat loss from the boundaries are negligible, therefore the boundaries are insulated. The initial conditions stem from the assumption that the specimen is at a constant temperature before the heating starts.

Two-temperature model with source term

The source term is included in the electron-energy equation

$$C_e \partial_t T_e = k \partial_x^2 T_e - G(T_e - T_\ell) + S. \quad (8.3.6)$$

From the three coupled equations, representing the two-temperature model, follows

$$\left(\frac{C_e C_\ell}{kG} \right) \partial_t^2 T + \left(\frac{C_e + C_\ell}{k} \right) \partial_t T = \partial_x^2 T + \left(\frac{C_\ell}{G} \right) \partial_t (\partial_x^2 T) + \frac{1}{k} S. \quad (8.3.7)$$

This equation (where $T = T_e = T_\ell$) governs either the lattice or the electron temperature.

Hyperbolic two-step (HTS) model with source term

So far, none of the models make provision for the electrons undergoing non-diffusive ballistic transport. This is a requirement to model femtosecond thermoreflectance measurements according to Nakamura *et al* ([NTYB11]). The hyperbolic two-step model fulfils this requirement by modifying the constitutive equation to have a form similar to that of the C-V model's constitutive equation

$$q = -k \partial_x T_e - \tau_F \partial_t q, \quad (8.3.8)$$

where τ_F is the thermalisation time of the electron gas [Dug16][Tzo95b], and $\tau_F \partial_t q$ represents the thermalisation stage in the electron gas. Combining the coupled equations associated with the HTS model, including the source term as in Eq. (8.3.6) leads to

$$\begin{aligned} \tau_F \left(\frac{C_e C_\ell}{kG} \right) \partial_t^3 T + \left(\frac{\tau_F (C_e + C_\ell)}{k} + \frac{C_e C_\ell}{kG} \right) \partial_t^2 T + \left(\frac{C_e + C_\ell}{k} \right) \partial_t T \\ = \partial_x^2 T + \left(\frac{C_\ell}{G} \right) \partial_t (\partial_x^2 T) + \frac{1}{k} (S + \tau_F \partial_t S). \end{aligned} \quad (8.3.9)$$

Second-order DPL model with source term

Tzou proposed a second-order DPL model, that according to him, correlates with the HTS model. This variation of the DPL model is based on the first-order effect in τ_T and the second-order effect in τ_q , so that the DPL constitutive equation becomes

$$q + \tau_q \partial_t q + \frac{\tau_q^2}{2} \partial_t^2 q = -k [\partial_x T + \tau_T \partial_t (\partial_x T)]. \quad (8.3.10)$$

Combining this constitutive equation with the energy equation, Eq. (8.3.2), yields the second-order DPL model equation

$$\begin{aligned} \frac{\tau_q^2}{2\alpha} \partial_t^3 T + \frac{\tau_q}{\alpha} \partial_t^2 T + \frac{1}{\alpha} \partial_t T \\ = \partial_x^2 T + \tau_T \partial_t (\partial_x^2 T) + \frac{1}{k} \left(S + \tau_q \partial_t S + \frac{\tau_q^2}{2} \partial_t^2 S \right). \end{aligned} \quad (8.3.11)$$

The model is therefore characterised by the addition of a third-order term describing the transient temperature response. The intention with second-order DPL model is to account for non-diffusive ballistic heat transfer in an electron gas.

Bibliography

- [AA15] H. Askarizadeh, H. Ahmadikia, Analytical study on the transient heating of a two-dimensional skin tissue using parabolic and hyperbolic bioheat transfer equations, *Appl. Math. Modelling* **39** (2015), 3704-3720.
- [AHZCB13] M. Akoshima, B. Hay, J. Zhang, L. Chapman, T. Baba, International Comparison on Thermal-Diffusivity Measurements for Iron and Isotropic Graphite Using the Laser Flash Method in CCT-WG9, *Int. Jnl. Thermophys* **34** (2013), 763-777.
- [AKP74] S. I. Anisimov, B. L. Kapeliovich, T. L. Perel'man, Electron emission from metal surfaces exposed to ultr-short laser pulses, *Sov. Phys. - JETP* **39**, (1974), 375-377.
- [Bab10] T. Baba, Measurements and data of thermophysical properties traceable to a metrological standard, *Metrologia* **47** (2010), S143-S155.
- [BCO81] E. B. Becker, G. F. Carey, J. T. Oden, *Finite elements. Volume I. An introduction*, The Texas Finite Element Series, I. Prentice-Hall Inc., Englewood Cliffs, NJ, (1981).
- [BDFW00] M. Bonn, D. N. Denzler, S. Funk, M. Wolf, S. S. Wellershoff, J. Hohlfeld, Ultrafast electron dynamics at metal surfaces: Competition between electron-phonon coupling and hot-electron transport, *Phys Rev B* **61**(2), (2000), 1101-1105.
- [BDV14] M. Basson, M. de Villiers, N. F. J. van Rensburg, Solvability of a Model for the Vibration of a Beam with a Damping Tip Body, *Jnl. Applied Mathematics Volume 2014*, Article ID 298092. <http://dx.doi.org/10.1155/2014/298092>
- [BFAPB12] E. Balčiūnas, G. Y. Fan, G. Andriukaitis, A. Pugžlys, A. Baltuška, High-power top-hat pulses from Yb master oscillator power

- amplifier for efficient optical parametric amplifier pumping, *Optics Letters* **37**(13) (2012), 2547-2549.
- [BFI62] S. D. Brorson, J. G. Fujimoto, E. P. Ippen, Femtosecond electronic heat transfer dynamics in thin gold film, *Phys. Rev. Lett.* **59**, (1987), 1962-1965.
- [BH69] K. J. Baumeister, T. D. Hamill, Hyperbolic heat conduction equation - a solution for the semi-infinite body problem, *ASME Jnl. of Heat Transfer* **91**, (1969), 543-548.
- [Bla74] J. S. Blakemore, *SOLID STATE PHYSICS" (SECOND EDITION)*, (1974), W B Saunders Company Philadelphia, London, Toronto.
- [Bro90] S. D. Brorson, *Femtosecond Thermomodulation Measurements of Transport and Relaxation in Metals and Superconductors*, RLE Technical Report No. 557 June 1990.
- [BSV17] M. Basson, B. Stapelberg, N. F. J. Van Rensburg, Error estimates for semi-discrete and fully discrete Galerkin finite element approximations of the general linear second order hyperbolic equation, *Numerical Function Analysis and Optimization* **38**(4), (2017), 466-485.
- [BTY11] T. Baba, N. Taketoshi, T. Yagi, Development of ultrafast laser flash methods for measuring thermophysical properties of thin films and boundary thermal resistances, *Jpn. Jnl. Appl. Physics* **50**, (2011), 11RA01.
- [BV13] M. Basson, N. F. J. Van Rensburg, Galerkin finite element approximation of general linear second order hyperbolic equations, *Numerical Function Analysis and Optimization* **34**(9), (2013), 976-1000.
- [BYTW10] T. Baba, N. Yamada, N. Taketoshi, H. Watanabe, M. Agoshima, T. Yagi, H. Abe, Y. Yamashita, Research and development of metrological standards for thermophysical properties of solids in the National Metrology Institute of Japan, *High Temperatures - High Pressures* **39**, (2010), 279-306.
- [Cat48] M. C. Cattaneo, Sulla conduzione de calore (On the conduction of heat), *Atti del Semin. Mat. e Fis. Univ. Modena* **3**(3), (1948), 83-101.
- [Cat58] M. C. Cattaneo, Sur une Frome de L'équation de la Chaleur Éliminant le Paradoxe D'une propagation Instantanée, *C. R. Acad. Sci. Paris Ser. I Math.* **247**, (1958), 431.

- [CDL77] C. Cohen-Tannoudji, B. Diu, F. Laloë, *Quantum Mechanics, Volume One*, Wiley-Interscience Publication, John Wiley & Sons (1977).
- [CT82] G. F. Carey, M. Tsai, "Hyperbolic heat transfer with reflection" *Num. Heat Transfer* **5**, (1982), 309-327.
- [CVV18] D. Civin, N. F. J. Van Rensburg, A. J. Van Der Merwe, "Using energy methods to compare linear vibration models", *Applied Mathematics and Computation*, **321** (2018) 602-613. <https://doi.org/10.1016/j.amc.2017.11.008>
- [CXW08] L. Cheng, M. Xu, L. Wang, "From Boltzmann transport equation to single-phase-lagging heat conduction", *Int. Jnl. Heat Mass Transfer* **51**, (2008), 6018-6023.
- [DA08] A. Soleimani Dorcheh, M. H. Abbasi, "Silica aerogel; synthesis, properties and characterization", *Journal of Materials Processing Technology* **199** (2008), 10-26.
- [DD19] B. Dekka, J. Dutta, Finite element methods for non-Fourier thermal wave model of bio heat transfer with an interface, *Inter. J. Appl. Math. Comput.*, doi.org/10.1007/s12190-019-01304-8, 2019.
- [Dug16] S. B. Dugdale, "Life on the edge: a beginner's guide to the Fermi surface", *Phys. Scr.* **91** (2016), 053009.
- [EGJA06] R. A. Escobar, S. S. Ghai, M. S. Jhon, C. H. Amon *et al*, "Multi-length and time scale thermal transport using the lattice Boltzmann method with application to electronics cooling", *Int. Jnl. Heat Mass Transfer* **49**, (2006), 97-107.
- [Eva98] L. C. Evans, "Partial differential equations", American Mathematical Society, 1998.
- [GK66] R. A. Guyer, J. A. Krumhansl, "Solution of the Linearized Boltzmann Equation", *Physical Review* **148**(3) (1966), 766-778.
- [HAA20] A. Hobiny, F. Alzahrani, I. Abbas, "Analytical estimation of temperature in living tissues using the TPL bioheat model with experimental verification", *Mathematics* **2020**, 8, 1188.
- [Hil62] S. Hildebrandt, "Rand- und Eigenwertaufgaben bei stark elliptischen Systemen linearer Differentialgleichungen", *Math. Analen*, **148**, 411-429.

- [HMWM97] J. Hohlfeld, J. G. Müller, S. S. Wellershof, E. Matthias, "Time-resolved thermorefectivity of thin gold films and its dependence on film thickness", *Applied Physics B* **64**, (1997), 387-390.
- [HN09] P. E. Hopkins, P. M. Norris, "Contribution of Ballistic Electron Transport to Energy Transfer During Electron-Phonon Nonequilibrium in Thin Metal Films", *Intl. Heat Transf.* **131**, April 2009, 043208-1–043208-8.
- [HW06] C. Huang, H. Wu, An inverse hyperbolic heat conduction equation problem in estimating surface heat flux by the conjugate gradient method, *J. Phys. D: Appl. Phys.* **39** (2006), 4087-4096.
- [Inm] D. J. Inman, "Engineering vibration", Prentice-Hall Inc, 1994, Englewood Cliffs, New Jersey.
- [JLZ02] F. Jiang, D. Liu, J. Zhou, Non-Fourier Heat Conduction Phenomena in Porous Material Heated by Microsecond Laser Pulse, *Microscale Thermophysical Engineering* **6** (2002), 331-346.
- [JO22] B. K. Jha, I. O. Oyelade, The role of dual-phase-lag (DPL) heat conduction model on transient free convection flow in an vertical channel, *Partial Differential Equations in Applied Mathematics* **5** (2022), 100266.
- [JP89] D.D. Joseph, L. Preziosi, Heat Waves , *Rev. Mod. Phys.* **61**(1) (1989), 41-73.
- [JP90] D.D. Joseph, L. Preziosi, Addendum to the paper 'Heat Waves', *Rev. Mod. Phys.* **62**(2) (1990), 375-391.
- [Kam90] W. Kaminski, "Hyperbolic Heat Conduction Equation for Materials With a Nonhomogeneous Inner Structure", *Jnl. Heat Transfer* **112**(3), (1990), 555-560.
- [KG07] K. Kim, Z. Guo, Multi-time-scale heat transfer modeling of turbid tissues exposed to short-pulsed irradiations, *Computer Methods and Programs in Biomedicine* **86** (2007), 112-123.
- [Kit05] C. Kittel, "Introduction to Solid State Physics" (Eighth Edition), (2005), John Wiley & Sons, Inc.
- [KKR16] D. Kumar, P. Kumar, K. N. Rai, "A study on DPL model of heat transfer in bi-layer tissues during MFH treatment", *Computers in Biology and Medicine* **75**, (2016), 160 - 172.

- [KLT57] M. I. Kaganov, I. M. Lifshitz, M. V. Tanatarov, "Relaxation between electrons and crystalline lattices", Soviet Physics JETP, Vol. 4, 173-178.
- [Kre89] E. Kreyszig, "Introductory Functional Analysis with Applications" (1989), John Wiley & Sons.
- [KSR16] D. Kumar, S. Singh, K. N. Rai, "Analysis of classical Fourier, SPL and DPL heat transfer model in biological tissues in presence of metabolic and external heat source", Heat and Mass Transfer **52**(6), (2016), 1098-1107.
- [Lam13] T. T. Lam, Int Jnl Heat and Mass Transfer 56 (2013), 653-666.
- [LC04] K. Liu, H. Chen, Numerical analysis for the hyperbolic heat conduction problem under a pulsed surface disturbance, Appl. Math. Comp. 159 (2004), 887-901.
- [LCP05] J. Li, P. Cheng, G.P. Peterson, J.Z. Xu, Rapid Transient Heat Conduction in Multilayer Materials with Pulsed Heating Boundary, Num. Heat Transf. A 47 (2005), 633-652.
- [LT20] A. Lakatos, A. Trnik, "Thermal Diffusion in Fibrous Aerogel Blankets", Energies **2020**, 13, 823.
- [Mai19] D. Maillet, "A review of the models using the Cattaneo and Vernotte hyperbolic heat equation and their experimental validation", Int. Jnl. Thermal Sciences **139** (2019), 424-432.
- [Max67] J. C. Maxwell, "On the Dynamical Theory of Gases", Phil. Trans. Royal Society of London, **157**, (1867), 49-88.
- [MF53] P. M. Morse and H. Feshbach, "Methods of Theoretical Physics", McGraw-Hill, New York, (1953).
- [MKVM95] K. Mitra, S. Kumar, A. Vedevarz and M. Moallemi, "Experimental Evidence of Hyperbolic Heat Conduction in Processed Meat", J. Heat Transfer **117**(3), (1995), 568-573.
- [MR16] T. N. Mishra, K. N. Rai, "Fractional single-phase-lagging heat conduction model for describing anomalous diffusion", Propulsion and Power Research **5**(1), (2016), 45-54.

- [MS21] E. Majchrzak, M. Stryczyński, Dual-phase lag model of heat transfer between blood vessel and biological tissue, *Mathematical Biosciences and Engineering* **18**(2) (2021), 1573-1589.
- [MT14] E. Majchrzak, L. Turchan, "A numerical analysis of heating tissue using the two-temperature model", *WIT Transactions on Engineering Sciences* **83**, (2014), 477 - 488.
- [Mul87] I. Müller, "ISIMM Kinetic theory and extended thermodynamics", *Symposium on Kinetic Theory and Extended Thermodynamics*, edited by I Müller and T Ruggeri (Pitagora Editrice, Bologna) (1987), 245.
- [MYSY21] J. Ma, X. Yang, Y. Sun, J. Yang, "Theoretical analysis on thermal treatment of skin with repetitive pulses", *Nature: Scientific Reports* (2021)11:9958.
- [NBB15] F. Nasri, M. F. Ben Aissa, H. Belmabrouk, Micoscale thermal conduction based on Cattaneo-Vernotte model in silicon on insulator and Double Gate MOSFETs, *Appl. Therm. Engineering* **76** (2015), 206-211.
- [NTYB11] F. Nakamura, N. Taketoshi, T. Yagi, T. Baba, "Observation of thermal transfer across a Pt thin film at a low temperature using a femtosecond light pulse thermoreflectance method", *Meas. Sci. Technol.* **22** (2011), 024013 (9pp).
- [OA12] J. Ordóñez-Miranda, J. J. Alvarado-Gil, "Determination of thermal properties for hyperbolic heat transport using a frequency-modulated excitation source", *Int. Jnl. Eng. Sci.* **50** (2012), 101-112.
- [OT94] M. N. Özisik, D. Y. Tzou, "On the Wave Theory in Heat Conduction", *Trans. ASME Jnl. Heat Transfer* **116**, (1994), 526-535.
- [Pat72] R. K. Pathria, "Statistical Mechanics", *International Series in Natural Philosophy Volume 45*, Pergamon Press Ltd, Headington Hill Hall, Oxford OX3 0BW, England.
- [PJBA61] W. J. Parker, R. J. Jenkins, C. P. Butler, G. L. Abbott, "Flash method of determining thermal diffusivity, heat capacity, and thermal conductivity", *Jnl. Appl. Phys.* **32** (1961), 1679-1684.
- [PR05] Y. Pinchover, J. Rubinstein, "An introduction to partial differential equations", Cambridge University Press, 2005.

- [PRDSS00] G. S. Prakash, S. S. Reddy, S. K. Das, T. Sundararajan, K. N. Seetharamu, "Numerical Modelling of Microscale Effects in Conduction for Different Thermal Boundary Conditions", *Num. Heat Transfer A* **38**, (2000), 513-532.
- [QT92] T. Q. Qiu, C. L. Tien, "Short-pulse laser heating on metals", *Int. Jnl. Heat Mass Transfer* **35**(3), (1992), 719-726.
- [QT93a] T. Q. Qiu, C. L. Tien, "Heat transfer mechanisms during short-pulse laser heating of metals", *ASME Jnl. Heat Transfer* **115**, (1993), 835-841.
- [QT93b] T. Q. Qiu, C. L. Tien, "Size effect on nonequilibrium laser heating of metals", *ASME Jnl. Heat Transfer* **115**, (1993), 842-847.
- [Ros90] H. M. Rosenberg, "The Solid State" (Third Edition), Oxford University Press, Walton Street, Oxford OX2 6DP, (1990).
- [RPD03] W. Roetzel, N. Putra, S. K. Das, "Experiment and analysis for non-Fourier conduction in materials with non-homogeneous inner structure", *Int. Jnl. Thermal Sciences* **42**, (2003), 541-552.
- [Sch71] M. Schechter, *Principles of functional analysis*, Academic Press, New York and London, 1971.
- [SF73] G. Strang, G. J. Fix, *An Analysis of the Finite Element Method*, Prentice-Hall, Englewood Cliffs, New Jersey, 1973.
- [Sho77] R. E. Showalter, "Hilbert space methods for partial differential equations". Pitman, London, 1977.
- [Sin94] R. K. Singh, "Target ablation characteristics during pulsed laser deposition of thin films" *Jnl. Non-Crystalline Solids* **178**, (1994), 199-209.
- [Sin10] N. Singh, "Two-Temperature Model of non-equilibrium electron relaxation: A Review", *Int. Jnl. Modern Physics B* **24**(09), (2010), 1141-1158.
- [SK20] S. K. Sharma, D. Kumar, "A Study on Non-Linear DPL Model for Describing Heat Transfer in Skin Tissue during Hyperthermia Treatment", *Entropy* **2020**, 22, 481.
- [Sos18] G. C. Sosso, "Understanding the Thermal Properties of Amorphous Solids Using Machine-Learning-Based Interatomic Potentials Molecular Simulation", Volume 44, 2018 - Issue 11: Machine Learning.

- [SS14] G. R. Ströher, G. L. Ströher, "Numerical thermal analysis of skin tissue using parabolic and hyperbolic approaches", *Int. Comm. Heat and Mass Transf.* **57**, (2014), 193-199.
- [SV11] R. H. Sieberhagen, N. F. J. van Rensburg, "Tracking a sharp crested wave front in hyperbolic heat transfer", *Appl. Math. Modelling* **36**(8), (2011), 3399-3410.
- [SVAIF94] C. K. Sun, F. Vallée, L. H. Acioli, E. P. Ippen, J. G. Fujimoto, "Femtosecond-tunable measurement of electron thermalization in gold", *Phys. Rev. B* **50**(20), (1994), 337-348.
- [SYS07] S. Z. Shuja, B. S. Yilbas, S. Z. Shazli, Laser repetitive pulse heating influence of pulse duty on temperature rise, *Heat Mass Transfer* **43** (2007), 949-955.
- [TA99] D. W. Tang, N. Araki, "Wavy, wavelike, diffusive thermal responses of finite rigid slabs to high-speed heating of laser-pulses", *Int. J. Heat Mass Transfer* **42** (1999), 855-860.
- [TBO99] N. Taketoshi, T. Baba, A. Ono, "Observation of heat diffusion across submicrometer metal thin films using a picosecond thermoreflectance technique", *Jpn. J. Appl. Phys.* **38** (1999), L1268-L1271.
- [TBO01] N. Taketoshi, T. Baba, A. Ono, "Development of a thermal diffusivity measurement system for metal thin films using a picosecond thermoreflectance technique", *Meas. Sci. Technol.* **12** (2001), 2064-2073.
- [TC94] C. L. Tien, G. Chen, "Challenges in microscale conductive and radiative heat transfer", *Jnl. Heat Transfer* **116**, (1994), 799-807.
- [TC01] D. Y. Tzou, K. S. Chiu, "Temperature-dependent thermal lagging in ultrafast laser heating", *Int. Jnl. Heat Mass Transfer* **44**, (2001), 1725-1734.
- [TM94] G. Tas, H. J. Maris, "Electron diffusion in metals studied by picosecond ultrasonics", *Phys. Rev. B* **49**(21) (1994), 15046-15054.
doi:10.3390/en11113163
- [TWZWO18] S. Tan, J. Wu, Y. Zhang, M. Wang, Y. Ou, A model of ultra-short pulsed laser ablation of metal with considering plasma shielding and non-Fourier effect, *Energies* **11** (2018), 3163.

- [TYB09] N. Taketoshi, T. Yagi, T. Baba, "Effect of Synthesis Condition on Thermal Diffusivity of Molybdenum Thin Films Observed by a Picosecond Light Pulse Thermoreflectance Method", *Jpn. J. Appl. Phys.* **48** (2009), Number 5S2.
- [TZ98] K. K. Tamma, X. Zhou, "Macroscale and microscale thermal transport and thermo-mechanical interactions: some noteworthy perspectives", *Jnl. Thermal Stresses* **21**, (1998), 405-449.
- [Tzo93b] D. Y. Tzou, "An engineering assessment to the relaxation time in thermal wave propagation", *Int. J. Heat Mass Transfer* **36(7)**, (1993), 1845-1851.
- [Tzo95a] D. Y. Tzou, "A Unified Field Approach for Heat Conduction from Macro- to Micro-Scales", *Trans. ASME Jnl. Heat Transfer* **117(9)**, (1995), 8-16.
- [Tzo95b] D. Y. Tzou, "The generalized lagging response in small-scale and high-rate heating", *Int. Jnl. Heat Mass Transfer* **38(17)**, (1995), 3231-3240.
- [Tzo95c] D. Y. Tzou, "Experimental support for the lagging behaviour in heat propagation", *Journal of Thermophysics and Heat Transfer* **9(4)**, (1995), 686-693.
- [Tzo97] D. Y. Tzou, "Macro- to Microscale Heat Transfer: The Lagging Behaviour", *Series in chemical and mechanical engineering*, Taylor and Francis, Washington (1997).
- [ULY21] T. Ullsperger, D. Liu, B. Y'urekli, G. Matth'aus, L. Schade, B. Seyfarth, H. Kohl, R. Ramm, M. Rettenmayr, S. Nolte, "Ultra-short pulsed laser powder bed fusion of Al-Si alloys: Impact of pulse duration and energy in comparison to continuous wave excitation", *Additive Manufacturing* **46** (2021), 102085.
- [Ver58a] P. Vernotte, *Les Paradoxes de la Théorie Continue de L'équation de la Chaleur*, *C. R. Acad. Sci. Paris Ser. I Math.*, **246** (1958), 3154-3155.
- [Ver58b] P. Vernotte, "La Véritable Équation de la Chaleur", *C. R. Acad. Sci. Paris Ser. I Math.*, **247**, (1958), 2103.
- [VS19] N. F. J. van Rensburg, B. Stapelberg, "Existence and uniqueness of solutions of a general linear second-order hyperbolic problem", *IMA Journal of Applied Mathematics* **84(1)**, (2019), 1-22.

- [VV02] N. F. J. Van Rensburg, A. J. Van Der Merwe, "Analysis of the solvability of linear vibration models", *Applicable Analysis* **81**(5), (2002), 1143-1159.
- [VVS21] A. J. Van Der Merwe, N. F. J. Van Rensburg, R. H. Sieberhagen, "Comparing the dual phase lag, Cattaneo-Vernotte and Fourier heat conduction models using modal analysis", *Appl. Math. Comp.* **396** (2021), 125934.
- [Wei95] H.F. Weinberger, *A First Course in Partial Differential Equations: with Complex Variables and Transform Methods*, Dover Publications Inc, New York (1995).
- [WHGM99] S. S. Wellershoff, J. Hohlfeld, J. Gdde, E. Matthias, "The role of electron-phonon coupling in femtosecond laser damage of metals", *Applied Physics A* **69**, (1999), S99-S107.
- [Win16] M. C. Wingert, "Thermal transport in amorphous materials: a review", *Semicond. Sci. Technol.* **31**(11), (2016), 113003.
- [WXZ01] L. Q. Wang, M. T. Xu, X. Zhou, "Well-posedness and solution structure of dual-phase-lagging heat conduction", *Int. Jnl. Heat Mass Transfer* **44**, (2001), 1659-1669.
- [YA20] H. M. Youssef, N. A. Alghamdi, "The exact analytical solution of the dual-phase-lag two-temperature bioheat transfer of a skin tissue subjected to constant heat flux", *Nature: Scientific Reports* (2020)10:15946.
- [YKN04] B. S. Yilbas, O. Khan, I. Z. Naqavi, Laser pulse heating and thermal stress developments: elastoplastic analysis, *Proceedings of the Institution of Mechanical Engineers Part B: Journal of Engineering Manufacture*, April 2004, 375-388.
- [Yil93] B. S. Yilbas, "Analytical solution for the heat conduction mechanism appropriate to the laser heating process", *Int. Comm. Heat Mass Transfer* **20**, (1993), 545-555.
- [Yil97] B. S. Yilbas, "Analytical solution for time unsteady laser pulse heating of semi-infinite solid", *Int. J. Mech. Sci.* **39**(6), (1997), 671-682.
- [Yil12] B. S. Yilbas, *Laser Heating Applications: Analytical Modelling*, Elsevier, 225 Wyman Street, Waltham, MA 02451, USA, First Edition (2012).

- [YS97a] B. S. Yilbas, S. Z. Shuja, "Heat transfer analysis of laser heated surfaces – conduction limited case" *Appl. Surf. Science* **108**, (1997), 167-175.
- [ZCG14] M. Zhang, B. Cao, Y. Guo, "Numerical studies on damping of thermal waves", *Int. Jnl. of Thermal Sciences* **84** (2014), 9-20.
- [ZCL17] Y. Zhang, B. Chen, D. Li, "Non-Fourier effect of laser-mediated thermal behaviors in bio-tissues: A numerical study by the dual-phase-lag model", **108**, (2017), 1428-1438.
- [Zei95] E. Zeidler, "Applied Functional Analysis: Applications to Mathematical Physics", Springer-Verlag, New York, 1995.
- [Zie77] O. C. Zienkiewicz, *The finite element method*, New York : McGraw-Hill, c1977, 3rd expanded and revised edition.
- [ZSY20] Q. Zhang, Y. Sun, J. Yang, "Bio-heat response of skin tissue based on three-phase-lag model", *Scientific Reports: Nature Research*, (2020) 10:16421.

Appendix A

Frequently used notation

Table A.1 includes frequently used or important mathematical notation, indicating where a definition or reference to it occurs in the thesis.

Table A.2 includes nomenclature associated with heat transfer and laser pulse parameters.

Table A.1: Mathematics notation

Symbol	Description	Section
Ω	n-dimensional bounded domain	4.2
$\partial\Omega$	Boundary of Ω	4.2
$(f, g)_\Omega$	Inner product: $(f, g)_\Omega = \int_\Omega fg$	4.3
J	Bounded or unbounded interval containing zero	4.4
$\mathcal{L}^2(\Omega)$	Square integrable functions	4.3
$u'(t) \in Y$	Weak partial derivative w.r.t. norm of Y	4.4
$H^m(\Omega)$	Sobolev space: the subspace of functions in $\mathcal{L}^2(\Omega)$ with weak partial derivatives up to order m	4.4

Table A.2: Physics notation

Symbol	Description
α	Thermal diffusivity
q	Heat flux
T	Temperature
τ	Relaxation time
τ_q	Lag time associated with q
τ_T	Lag time associated with ∇T
t	Time
d	Length
t_d	Heat diffusion time
$t_{1/2}$	Half-time
t_p	Pulse width
τ_p	Pulse period
r_d	Duty ratio: $r_d = t_p/\tau_p$